Bioorg. Med. Chem. 114 (2024) 117958

Contents lists available at ScienceDirect

Bioorganic & Medicinal Chemistry

journal homepage: www.elsevier.com/locate/bmc

Novel benzenesulfonamide-aroylhydrazone conjugates as carbonic anhydrase inhibitors that induce MAPK/ERK-mediated cell cycle arrest and mitochondrial-associated apoptosis in MCF-7 breast cancer cells

Beata Żołnowska [a,*], Jarosław Sławiński [a], Jarosław Chojnacki [b], Andrea Petreni [c], Claudiu T. Supuran [c], Anna Kawiak [d,**]

[a] Department of Organic Chemistry, Medical University of Gdańsk, Al. Gen. J. Hallera 107, 80-416 Gdańsk, Poland
[b] Department of Inorganic Chemistry, Gdańsk University of Technology, ul. Narutowicza 11/12, 80-233 Gdańsk, Poland
[c] Università degli Studi di Firenze, NEUROFARBA Dept., Sezione di Scienze Farmaceutiche, 50019 Sesto Fiorentino (Florence), Italy
[d] Intercollegiate Faculty of Biotechnology, University of Gdańsk and Medical University of Gdańsk, ul. Abrahama 58, 80-307 Gdańsk, Poland

ARTICLE INFO

Keywords:
Anticancer
Apoptosis
Benzenesulfonamide
Carbonic anhydrase
Cell cycle arrest
MAPK/ERK pathway
Synthesis

ABSTRACT

A series of novel 4-alkylthio-2-chloro-5-[(2-arylmethylidene)hydrazinecarbonyl]benzenesulfonamide derivatives **3–22** were synthesized and evaluated for their inhibitory activity against human carbonic anhydrase isozymes hCA I, hCA II, hCA IX, and hCA XII. These compounds showed varying degrees of activity against the studied isoenzymes. However, the importance of substituent choice in designing potent carbonic anhydrase inhibitors is highlighted by the strong inhibition profiles of compounds **3** and **10** against hCA IX and the low average K_I values for compounds **9** and **10** (134 nM and 77 nM, respectively). All the synthesized compounds were evaluated for their antiproliferative activity toward HeLa, HCT-116, and MCF-7 cell lines. Compounds **9** and **19** exhibited significant activity, particularly against the MCF-7 cell line (IC_{50} values of 4 μM and 6 μM, respectively). Notably, compound **9** demonstrated a high selectivity index (SI = 8.2) for MCF-7 cells. The antiproliferative effects of compounds **9** and **19** were linked to the induction of cell cycle arrest and apoptosis via the mitochondrial pathway and involved the activation of the MAPK/ERK signaling pathway. Inhibition of MAPK/ERK activity reduced the compounds' ability to induce cell cycle arrest and apoptosis, indicating the critical role of this pathway. These findings suggest that compounds **9** and **19** are promising candidates for further development as specific and potent anticancer agents targeting the MAPK/ERK pathway.

1. Introduction

Apoptosis, or programmed cell death, is critical mechanism for maintaining cellular homeostasis by eliminating damaged cells. Dysregulation of this process can lead to the uncontrolled proliferation of abnormal cells, contributing to cancer development. Impaired apoptosis has been implicated not only in the initiation but also in therapy resistance across many cancers, including breast cancer.[1,2] As one of the leading causes of death among women, the lifetime risk of being diagnosed with invasive breast cancer in the U.S. is estimated to be about 13 %. The incidence of breast cancer is increasing by 0.5 % annually, driven by the detection of localized and hormone receptor-positive subtypes.[3] This highlights the need for ongoing research into treatments that can selectively restore apoptotic mechanisms in these cancer cells.

Various intercellular signaling pathways are involved in the regulating cell cycle arrest and apoptosis. The Mitogen-Activated Protein Kinase/Extracellular Signal-Regulated Kinase pathway (MAPK/ERK) is pivotal in the regulation of these processes. In particular, the ERK protein, one of the most extensively studied MAPKs, controls a wide subset of cellular targets involved in survival and cell death regulation. ERK can directly phosphorylate proteins involved in apoptosis regulation, including anti-apoptotic and pro-apoptotic Bcl-2 family proteins. Through the regulation of transcription factors, ERK controls the expression of genes involved in cell cycle progression, such as cyclins

* Corresponding author at: Department of Organic Chemistry, Medical University of Gdańsk, Al. Gen. J. Hallera 107, 80-416 Gdańsk, Poland.
** Corresponding author at: Intercollegiate Faculty of Biotechnology, University of Gdańsk and Medical University of Gdańsk, ul. Abrahama 58, 80-307 Gdańsk, Poland.
E-mail addresses: zolnowska@gumed.edu.pl (B. Żołnowska), anna.kawiak@biotech.ug.edu.pl (A. Kawiak).

https://doi.org/10.1016/j.bmc.2024.117958
Received 21 August 2024; Received in revised form 23 September 2024; Accepted 8 October 2024
Available online 15 October 2024

and cyclin-dependent kinases (CDKs).[4,5] These regulatory mechanisms emphasize the importance of understating the involvement of ERK in mediating cell fate. Furthermore, delineating the mechanisms involved in cell death regulation is important in developing effective therapeutic strategies.

Sulfonamides constitute a classic group of chemotherapeutic drugs with a broad spectrum of pharmacological action. Historically, this class of compounds derives from the simple sulfanilamide which was the leading structure for development of important drugs such as antibacterial sulfathiazole,[6] antiglaucoma acetazolamide,[7] diuretic furosemide,[8] hypoglycemic agent glibenclamide[9] or antiviral amprenavir.[10] Reports indicate that sulfonamide derivatives demonstrate in vitro and in vivo antitumor activity with various mechanisms of action, such as carbonic anhydrase inhibition, cell cycle perturbation in G1 phase, inhibition of tubulin polymerization or angiogenesis inhibition (inhibition of extracellular matrix metalloproteinases).[11] Sulfonamide scaffolds are also known to modulate various kinases such as ACK1/TNK, LMTK3, and EGFR overexpressed in different types of cancer including breast cancer.[12]

Sulfonamides are also the largest class of carbonic anhydrase (CA) inhibitors. The CA inhibition mechanism by sulfonamides involves binding of the sulfonamide group to the Zn^{2+} ion which is located in the active center of the enzyme. The sulfonamide residue is often attached to an aromatic or heterocyclic ring.[13]

Carbonic anhydrases (CAs, EC 4.2.1.1), zinc-containing enzymes, are pivotal enzymes catalyzing the hydration of carbon dioxide, crucial for maintaining biochemical equilibrium and cellular acid-base homeostasis.[13] CAI and CAII are overexpressed in a variety of tumors, and their overexpression has often been correlated with the aggressiveness of tumor cells, such as for example in colorectal cancer and synchronous distant metastasis.[14] Carbonic anhydrases IX, and XII occur mainly in neoplastic cells and show limited expression in normal tissues. These isoforms have been shown to cause acidification of solid tumors by hydration of carbon dioxide to a proton and bicarbonate.[15–17] The use of CA IX and XII inhibitors partially inhibits this phenomenon.[18,19] CA isoforms IX and XII are highly overexpressed in many neoplastic tissues in response to the hypoxia-inducing factor (HIF) activation cascade. Research on the participation of CA IX and XII in the processes of carcinogenesis has developed significantly in recent years,[20] with interesting results that demonstrated not only their role in the microenvironment but also their involvement in ferroptosis and metastases inhibition.[21,22]

Hydrazone and its derivatives with azomethine —CH═NNH— group belong to an important class of compounds with diverse biological and pharmacological activities such as anti-inflammatory, antibacterial, analgesic, antifungal, anti-hypertensive, antiplatelet, antiviral, antimalarial, antidepressant, anticonvulsant and anticancer, etc.[23,24] In particular, aroylhydrazones pay special attention due to their especially high and selective antiproliferative activities.[25–28] In addition to the extended biological properties of hydrazones, they are also combined with other pharmacophores to provide pharmacologically active molecules.

The new sulfonamide derivatives were designed as molecular conjugates of a 4-alkylthiobenzenesulfonamide fragment **A** (Fig. 1) and various arylhydrazones substituted with electron-withdrawing and donating substituents or heteroarylhydrazones **B** (Fig. 1) to investigate the influence of the structural features of compounds on their antiproliferative activity. The cytotoxic activity of the benzenesulfonamides was assessed toward breast, cervical, and colorectal cancer cell lines representing some of the most common cancers. Breast cancer is the most frequently diagnosed cancer in women worldwide and is the leading cause of cancer death among women worldwide (2 308 897 new cases, 665 684 cancer deaths in 2022).[29] The compounds with the highest activity were further examined, and their mechanism of action was delineated in breast cancer cells, which exhibited the highest sensitivity to the benzenesulfonamides. The ability of compounds to induce apoptosis and cell cycle arrest was evaluated, and the role of MAPK/ERK in these processes was examined.

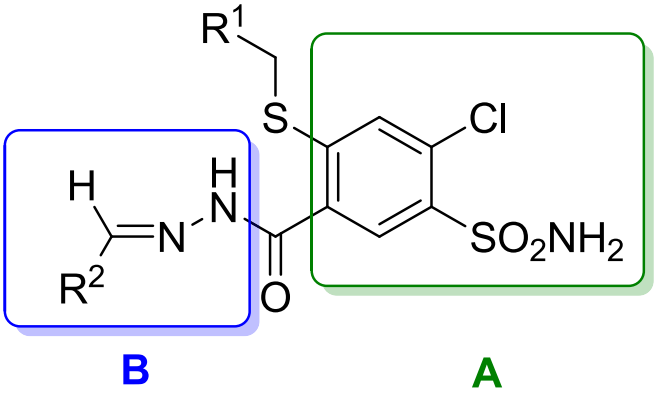

Fig. 1. General structure of molecular conjugates of a 4-alkylthiobenzenesulfonamide fragment (**A**) and various aryl/heteroarylhydrazones (**B**).

2. Results

2.1. Chemistry

The starting substrates **1** and **2** were obtained by a reaction of 2,4-dichloro-5-sulfamoylbenzohydrazide with benzylthiol or 4-fluorophenylmethanethiol in the presence of tetrabutylammonium iodide (TBAI), potassium carbonate (K_2CO_3) in an acetonitrile/water mixture (Scheme 1).

The final products **3–22** were synthesized by heating substrate **1** or **2** with the appropriate aldehydes in the presence of catalytic amount of sulfuric acid, in ethanol for 0.5–2.5 h (Scheme 2). The products were obtained with yield in the range of 38–95 %.

The chemical structure of the new compounds **2–22** was confirmed by spectroscopic methods – IR, ^{1}H NMR, and HRMS. Additionally, elemental analysis (C, H, N) was performed for all compounds. X-Ray crystallographic analysis was performed on a representative compound **3**.

^{1}H-NMR spectra confirmed the chemical structure of compounds **2–22.** In the range of 4.26–4.43 ppm, a singlet with integration of two protons, originating from the CH_2-S group, was observed. In the range of 6.15–9.02 ppm, multiplets of varying integration were visible, originating from aromatic protons and the SO_2NH_2 group. Among the protons of the aromatic system, two singlets were distinguished with the integration of one proton for each singlet – the signal corresponding to the H-3 proton was in the range of 7.56–7.71 ppm, while the singlet assigned to the H-6 proton was in the range of 7.90–8.07 ppm. Moreover, in the range of 8.23–8.47 ppm there was a singlet with the integration of one proton assigned to the N═CH group, while in the range of 9.46–12.62 ppm there was a singlet with the integration of one proton assigned to the NH group.

X-Ray analysis showed *E* conformation for a hydrazone function in benzenesulfonamide-aroylhydrazone conjugates. Compound **3** formed transparent needle crystals satisfying symmetry of the monoclinic system, the space group $P2_1/c$ (no. 14). Asymmetric unit contains one molecule and the whole unit cell contains four molecules of the sulfonamide, Z = 4. Most of the bond lengths and angles are in the expected ranges. Crystal data, data collection and structure refinement details are summarized in Table 1S (Supplementary material). Molecular structure and atom labeling scheme are given in Fig. 2. Details on hydrogen bonding are gathered in Table 2S (Supplementary material). Notably oxygen atoms from the sulfonamide group do not participate in hydrogen bonding. This may indicate the sulfonamide group is not ionized. Instead, hydrogen bonding of the NH…O and NH…N are present in the structure, which allows formation of infinite chains

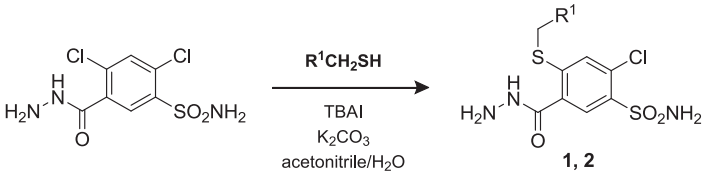

Compound	R^1
1	Ph
2	4-FPh

Scheme 1. Synthesis of substrates – 4-alkylthio-2-chloro-5-(hydrazinecarbonyl)benzenesulfonamides: a) R^1CH_2SH (1 equiv.), tetrabutylammonium iodide (1 equiv.), K_2CO_3 (2.1 equiv.), acetonitrile/water (v/v = 100/1), 24 h r.t.

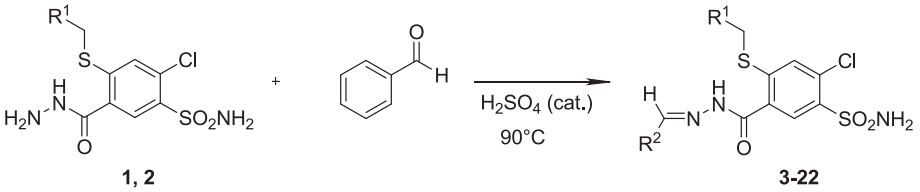

Compd	R^1	R^2
1, 3	Ph	4-ClPh
1, 4	Ph	4-BrPh
1, 5	Ph	4-FPh
1, 6	Ph	Ph
1, 7	Ph	4-NO_2Ph
1, 8	Ph	4-CF_3Ph
1, 9	Ph	2-OH-4-BrPh
1, 10	Ph	2-OH-4-OHPh
1, 11	Ph	2-quinolinyl
1, 12	Ph	4-pyridyl
2, 13	4-FPh	4-ClPh
2, 14	4-FPh	4-BrPh
2, 15	4-FPh	4-FPh
2, 16	4-FPh	Ph
2, 17	4-FPh	4-NO_2Ph
2, 18	4-FPh	4-CF_3Ph
2, 19	4-FPh	2-OH-4-BrPh
2, 20	4-FPh	2-OH-4-OHPh
2, 21	4-FPh	2-quinolinyl
2, 22	4-FPh	4-pyridyl

Scheme 2. Synthesis of 4-alkylthio-2-chloro-5-[(2-arylmethylidene)hydrazinecarbonyl]benzenesulfonamide derivatives: a) ethanol, one drop of H_2SO_4 conc., 90 °C, 0.5–2.5 h.

propagating parallel to the crystallographic **c** vector (direction [0 0 1]). Character of the double bond for C15=N3 is confirmed by its short length. Crystal packing and hydrogen bonding in **3** are shown in Fig 3.

2.2. CA inhibition studies

The compounds **3**–**22** and standard, clinically used CAI, acetazolamide **AAZ**, were screened for the inhibition of two cytosolic ubiquitous isozymes of human origin hCA I and hCA II, and transmembrane tumor-associated isoforms hCA IX and XII (Table 1). From the inhibition data reported in Table 1, the following points were noticed and presented in Fig 4:

- K_I hCA I showed the lowest affinity to tested compounds. Only **18** and **20** were able to inhibit this isoform with K_I about 80 nM.
- The majority of 4-benzylthio-2-chloro-5-[(2-arylmethylidene)-hydrazinecarbonyl]benzenesulfonamides effectively inhibited hCA II in the range of K_I values from 23.5 nM to 76.7 nM. Comparing the substituents R^1, it can be noticed that for better inibitory effect phenyl group is prefered. Moreover the highest affinity is given by **4** including phenyl group as R^1 and 4-bromophenyl moiety in R^2 substituent. Compound **4** (K_I = 23.5 nM) stands out with high potency, comparable to the reference drug AAZ. More electronegative atoms such as chlorine (**3**) and fluorine (**5**) in substituent R^2 redcued inhibitory activity threefold.
- The most potent inhibitors of hCA IX showing K_I about 58 nM include R^1 = Ph and R^2 = 4-ClPh (**3**) or 2-OH-4-OHPh (**10**).
- In the case of hCA IX inhibition, a similar trend to hCA II was observed, namely higher inhibitory activities were observed for derivatives with R^1 = Ph. With the exception of three compounds (**7, 8, 11**), the K_I values ranged from 57.7 to 95.7 nM.
- Compound **3** (K_I = 57.7 nM) demonstrates strong inhibition, closely following the performance of SLC-0111.
- Inhibition of the hCA XII isoform showed a similar tendency as for hCA II and IX, with K_I values ranging from 50.7 to 90.4 nM. The highest activity was exhibited by compound **12**.

The data highlight the importance of substituent choice in designing potent carbonic anhydrase inhibitors. Compounds **3** and **10**, with their strong inhibition profiles for hCA IX, present promising leads for further development. Additionally, compound **9** ($K_{I\ average}$ = 134 nM) and **10** ($K_{I\ average}$ = 77 nM) show promising inhibition profiles with low average K_I values, making them strong candidates for further research. Future studies should focus on optimizing these lead compounds for improved

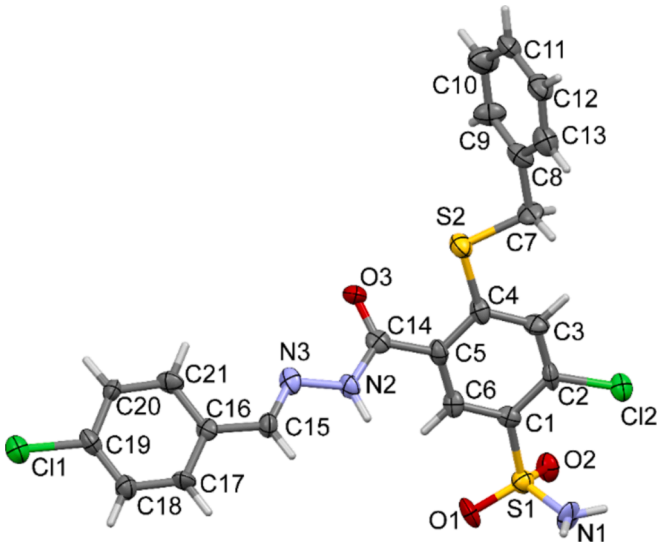

Fig. 2. ORTEP diagram of compound **3**, showing atom labelling scheme. Displacement ellipsoids are shown at 50 % probability. Selected bond lengths (Å) and angles (°): S1-N1 1.600(8), S1-O1 1.446(6), S1-O2 1.440(6), S1-C1 1.765(10), N2-N3 1.414(10), N2-C14 1.368(11), N3-C15 1.290(11), O3-C14 1.243(11); N1-S1-C1 108.3(5), C4-S2-C7 102.0(5), C8-C7-S2 108.3(7), C14-N2-N3 118.4(8), C15-N3-N2 113.2(8), O3-C14-C5 123.2(9), O3-C14-N2 121.9(9).

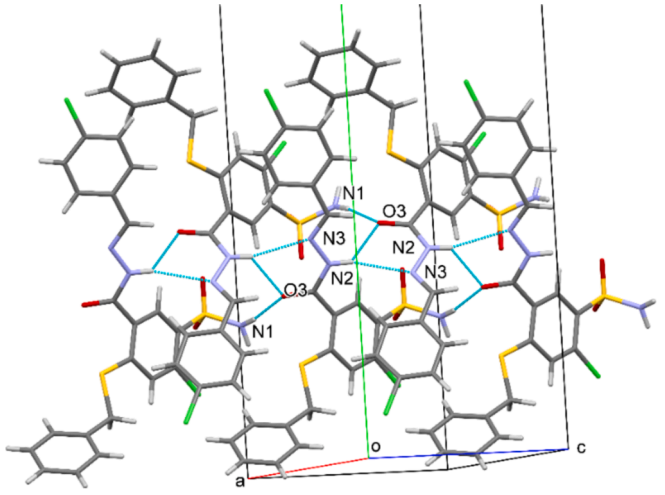

Fig. 3. Crystal packing and hydrogen bonding in **3**. Molecules are linked by hydrogen bonding of the NH..O and NH…N type, forming infinite chains propagating along crystallographic [0 0 1] direction. Both donor types —$SO_2N\mathbf{H}_2$ and —*N*-N**H**=C are used in hydrogen bonding (drawn as dashed blue lines). (For interpretation of the references to colour in this figure legend, the reader is referred to the web version of this article.)

specificity and potency.

2.3. Cell viability

Compounds **1**–**22** were tested for their cytotoxic activity toward three cancer cell lines: HCT-116 (colon cancer), HeLa (cervical cancer), and MCF-7 (breast cancer). HaCaT, the human keratinocyte cell line, was used as the control cell line. The analysis was performed using the MTT assay, and the results are presented in Table 2, expressed as IC_{50} values. Cisplatin was used as a positive drug control.

The results of the MTT assay showed that the HCT-116 cell line demonstrated the highest sensitivity toward the benzenesulfonamide

Table 1
Carbonic anhydrase inhibition data for compounds **3**–**22** and standard inhibitors against human isozymes hCA I, II, IX and XII by a stopped-flow CO_2 hydrase assay.

Compound	R^1	R^2	CA I	CA II	CA IX	CA XII
				K_I (nM)[a]		
3	Ph	4-ClPh	589.6	**76.1**	**57.7**	**88.7**
4	Ph	4-BrPh	425.2	**23.5**	**95.7**	258.4
5	Ph	4-FPh	3947	**76.7**	**72.9**	**90.4**
6	Ph	Ph	386.4	**35.6**	**93.3**	777.9
7	Ph	4-NO_2Ph	3581	300.0	892.0	5114
8	Ph	4-CF_3Ph	2185	271.9	826.1	879.0
9	Ph	2-OH-4-BrPh	328.2	**41.1**	**85.7**	**82.2**
10	Ph	2-OH-4-OHPh	144.3	**49.1**	**58.1**	**56.8**
11	Ph	2-quinolyl	8939	2818	7576	6920
12	Ph	4- pyridyl	635.6	**61.6**	**74.4**	**50.7**
13	4-FPh	4-ClPh	8308	7218	7795	1820
14	4-FPh	4-BrPh	5265	3121	8149	1914
15	4-FPh	4-FPh	892.9	669.1	696.6	421.6
16	4-FPh	Ph	917.6	512.2	692.1	667.6
17	4-FPh	4-NO_2Ph	8427	6889	7474	2692
18	4-FPh	4-CF_3Ph	**87.2**	952.6	887.5	237.8
19	4-FPh	2-OH-4-BrPh	537.2	646.4	851.8	695.1
20	4-FPh	2-OH-4-OHPh	**80.7**	**56.1**	**80.1**	**80.3**
21	4-FPh	2- quinolyl	7358	837.5	5899	781.3
22	4-FPh	4-pyridyl	6099	868.5	6784	677.8
AAZ			250.0	12.0	25.0	5.7
SLC-0111[b]			5080	960	45	4.5

K_I values < 100 nM in bold type.
[a] Mean from 3 different assays, by a stopped flow technique (errors were in the range of ± 5–10 % of the reported values).
[b] 30.

derivatives. Among the examined compounds, seven displayed significant activity, with two compounds showing high activity (**9, 19**; $IC_{50} = 6$ μM), and five moderate activity (**2, 8, 10, 18, 20**; IC_{50} in the range of 11.0–18 μM). In the case of the MCF-7 cell line, four compounds exhibited significant cytotoxic activity. Compounds **9** and **19** showed high activity (**9,** $IC_{50} = 4$ μM**; 19**, $IC_{50} = 6$ μM), while compounds **8** and **18** showed moderate activity, both displaying an IC_{50} value of 18 μM. The lowest activity was noted toward the HeLa cell line, where three compounds, **9, 18,** and **19,** showed moderate cytotoxicity – IC_{50} in the range of 14–18 μM.

The high selectivity of an active substance is a property highly desirable for a potential anticancer drug. Higher cytotoxicity toward cancer cells than toward non-malignant cells significantly reduces the incidence of side effects of chemotherapy. It is worth emphasizing that compounds with significant anti-proliferative activity (**2, 8–10, 18–20**) showed lower cytotoxicity toward control HaCaT cells in comparison to cancer cells (Table 2). The highest selectivity was demonstrated by compounds **9, 18,** and **19**, with selectivity indices (SI) ranging from 5.5 to 8.2, and the highest SI value was established for compound **9** toward MCF-7 cells (Table 3).

The compounds exhibiting the highest activity along with the highest selectivity, compounds **9** and **19**, were selected for further analysis of their mechanism of action. The time-dependent inhibitory effects of these compounds on MCF-7 cell proliferation were assessed following a 24-, 48-, and 72-hour incubation period. After 24 h of incubation, the IC_{50} values of compounds **9** and **19** were 98 μM and 90 μM, respectively. A further 24 h incubation period significantly reduced the IC_{50} values of both compounds to 6 μM. After a 72-h incubation, the results of the MTT assay indicated higher activity of compound **9** with a further decrease in the IC_{50} value of compound **9** to 4 μM, whereas the activity of compound **19** remained the same (Fig. 5**A**).

The long-term effects of compounds **9** and **19** on MCF-7 cells were examined with the colony-forming assay. This assay examines the capability of individual cells to grow into colonies, providing insight into the ability of the compounds to inhibit the clonogenicity of cells. The colony-forming assay was assessed after a 24-hour treatment of cells

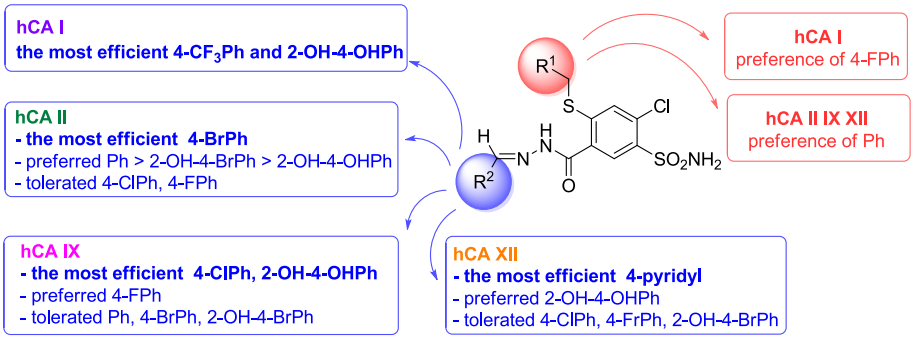

Fig. 4. Structure-activity relationship of benzenesulfonamide-aroylhydrazone conjugate.

Table 2
Antiproliferative activity of compounds **1**–**22** assessed by the MTT test[a] and expressed by IC_{50} values.

Compound	R^1	R^2	HCT-116	HeLa	MCF-7	HaCaT
				IC_{50} [μM]		
1	Ph	–	155 ± 9	350 ± 14	105 ± 6	n.t.
2	4-FPh	–	**18 ± 0.5**	36 ± 1	24 ± 1	65 ± 3
3	Ph	4-ClPh	23 ± 1	28 ± 1	34 ± 1	225 ± 11
4	Ph	4-BrPh	23 ± 1	26 ± 0.3	26 ± 0.5	80 ± 3
5	Ph	4-FPh	23 ± 0.5	23 ± 1	25 ± 0.5	150 ± 8
6	Ph	Ph	48 ± 1	67 ± 5	49 ± 1	83 ± 3
7	Ph	4-NO_2Ph	95 ± 6	69 ± 3	30 ± 1	>500
8	Ph	4-CF_3Ph	**18 ± 1**	23 ± 1	**18 ± 0.5**	54 ± 2
9	Ph	2-OH-4-BrPh	**6 ± 0.2**	**16 ± 1**	**4 ± 0.2**	33 ± 1
10	Ph	2-OH-4-OHPh	**14 ± 0.5**	29 ± 0,6	22 ± 0.5	58 ± 2
11	Ph	2-quinolyl	31 ± 2	38 ± 2	31 ± 2	84 ± 4
12	Ph	4-pyridyl	81 ± 3	95 ± 6	90 ± 5	n.t.
13	4-FPh	4-ClPh	24 ± 0.5	28 ± 1	27 ± 1	350 ± 18
14	4-FPh	4-BrPh	110 ± 6	110 ± 4	73 ± 2	n.t.
15	4-FPh	4-FPh	120 ± 6	105 ± 4	86 ± 3	n.t.
16	4-FPh	Ph	150 ± 8	140 ± 8	115 ± 5	n.t.
17	4-FPh	4-NO_2Ph	73 ± 3	76 ± 4	137 ± 7	n.t.
18	4-FPh	4-CF_3Ph	**11 ± 0.3**	**14 ± 0.5**	**18 ± 0.5**	68 ± 2
19	4-FPh	2-OH-4-BrPh	**6 ± 0.2**	**18 ± 1**	**6 ± 0.3**	33 ± 1
20	4-FPh	2-OH-4-OHPh	**11.5 ± 0.4**	28 ± 1	25 ± 1	32 ± 1
21	4-FPh	2-quinolyl	35 ± 2	38 ± 2	37 ± 2	165 ± 8
22	4-FPh	4-pyridyl	67 ± 3	91 ± 2	61 ± 2	550 ± 33
Cisplatin	–	–	**3.8 ± 0.2**	**2.2 ± 0.1**	**3.0 ± 0.1**	**7.7 ± 0.2**

[a] Analysis was performed using the MTT assay after 72 h of incubation and the results are expressed as IC_{50} values (indicating a 50 % reduction in cell proliferation) – Values are expressed as the mean ± SD of at least three independent experiments.
n.t.-not tested, **IC_{50}** values <20 μM are in bold type.

Table 3
Selectivity indexes (SI) of selected compounds toward cancer cells.

Compound	R^1	R^2	HCT-116	HeLa	MCF-7
			Selectivity indices (SI)		
2	4-FPh	–	3.6	1.8	2.7
8	Ph	4-CF_3Ph	3.0	2.3	3.0
9	Ph	2-OH-4-BrPh	5.5	2.0	8.2
10	Ph	2-OH-4-OHPh	4.1	2.0	2.6
18	4-FPh	4-CF_3Ph	6.1	4.8	3.7
19	4-FPh	2-OH-4-BrPh	5.5	1.8	5.5
20	4-FPh	2-OH-4-OHPh	2.9	1.1	1.2

Selectivity indices: IC_{50} value toward HaCaT cells/ IC_{50} value toward cancer cells.

following re-seeding of cells at a low density and a 2-week incubation period. In line with the MTT assay, the results of the colony-forming assay indicated higher anti-proliferative activity of compound **9**, which at the concentration of 2.5 μM reduced colony formation by 80 %. In contrast, the reduction of colony formation by compound **19** at this concentration was 65 %. At the concentration of 5 μM, a significant decrease in the clonogenic potential of MCF-7 cells was observed in the case of both compounds, decreasing colony formation by 85 % and 80 % by compounds **9** and **19**, respectively (Fig. 5**B**).

2.4. Cell cycle distribution and apoptosis analysis

To determine whether cell proliferation inhibition is associated with perturbations in the cell cycle, the analysis of cell cycle distribution was performed following treatment with compounds **9** and **19**. Cells were incubated with the compounds in the concentration range of 2.5 μM–10 μM for 48 h and 72 h, and analysis was performed using flow cytometry. The results indicated the induction of cell cycle arrest by both compounds at the lower concentrations examined. At the concentration of 2.5 μM, an increase in the G2/M population of cells was observed, whereas at 5 μM, S phase arrest was induced. At the higher examined concentration of 10 μM, an increase in the sub-G1 population was determined, indicating a possible transition to apoptosis. At 72 h of incubation, a lower increase in the G2/M and S phase was noted, with a higher increase in the sub-G1 population of cells (Fig. 6), pointing to a shift from cell cycle inhibition to apoptosis at higher concentrations and longer incubation periods.

The increase in the sub-G1 population indicated possible apoptosis induction, which was verified by assessing the ability of compounds **9** and **19** to induce phosphatidylserine externalization in MCF-7 cells. Cells were treated for 72 h with compounds **9** and **19** in the concentration range of 2.5 μM–10 μM. Flow cytometry analysis with Annexin V staining showed the ability of both compounds to induce apoptosis in a concentration-dependent manner. Both early and late apoptotic cell populations were induced upon compound treatment, with the predominant induction of the late apoptotic over the early apoptotic

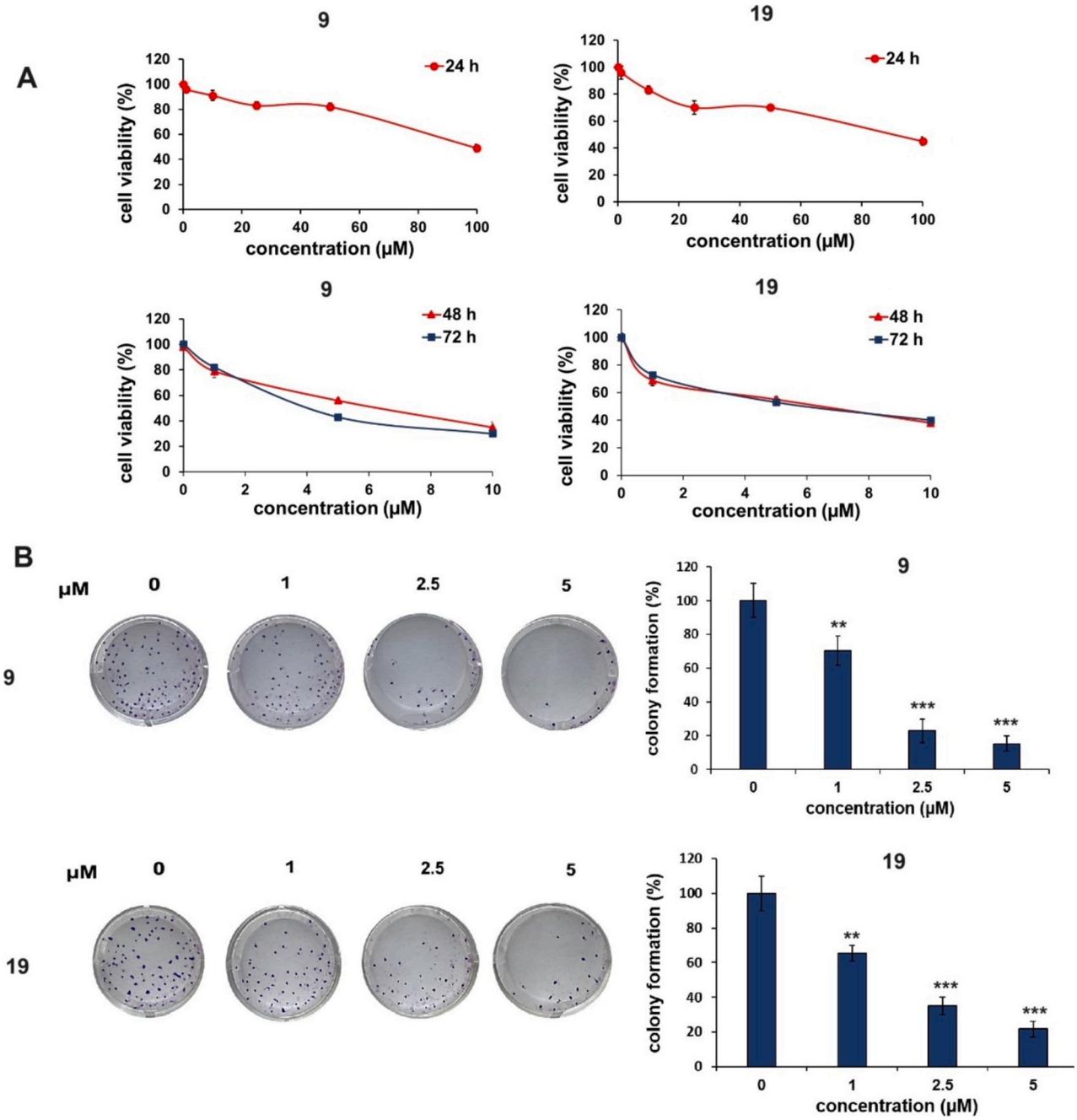

Fig. 5. Inhibition of MCF-7 cell proliferation by compounds **9** and **19**. (**A**) Time-dependent inhibition of the cell viability of MCF-7 cells following 24, 48, and 72 h of incubation with compounds **9** and **19.** Cells were treated with the indicated concentrations, and cell viability was determined with the MTT assay. (**B**) The inhibition of colony formation by compounds **9** and **19**. Cells were treated with the indicated concentrations of compounds **9** and **19** for 24 h, and after a 2-week incubation, colonies were stained with crystal violet. Values are means ± SD of three independent experiments. Data were analyzed by one-way ANOVA with Tukey's post hoc test, $p < 0.01$ (**), $p < 0.001$ (***). (For interpretation of the references to colour in this figure legend, the reader is referred to the web version of this article.)

population. At the highest examined concentration of 10 μM, compounds **9** and **19** increased the total apoptotic population to 65 % and 60 %, respectively (Fig. 7**A**). The involvement of the mitochondrial pathway in apoptosis induction was further verified. The changes in mitochondrial membrane potential (Δψm) were assessed by flow cytometry with JC-1 cell staining, following treatment of cells for 48 h with compounds **9** and **19**. The loss of Δψm, as shown by a decrease of accumulated JC-1 aggregates in the mitochondria and an increase in JC-1 cytoplasmic monomers, was induced in a concentration-dependent manner. The highest loss of Δψm was observed at 10 μM and increased to 40 % and 30 % by compounds **9** and **19**, respectively (Fig. 7**B**). The loss of Δψm triggers a cascade of events leading to cell death, which include the proteolytic cleavage and activation of the caspase cascade. In order to determine caspase activation by compounds **9** and **19**, cells following a 48-h treatment were incubated with a carboxyfluorescein-labeled caspase inhibitor, which targets multiple caspases (1, 2, 3, 6, 7, 8, 9, 10, 13), and fluorescent intensity was assessed with flow cytometry. The caspase inhibitor, through binding with active caspases, inhibits their activity and enables the quantification of caspase activity by measuring the intensity of the fluorescent signal of the bound inhibitor. The use of a pan-caspase inhibitor allowed to broadly confirm caspase involvement in apoptosis induced by the examined compounds. The results showed that compounds **9** and **19** induced a concentration-dependent increase in caspase activity

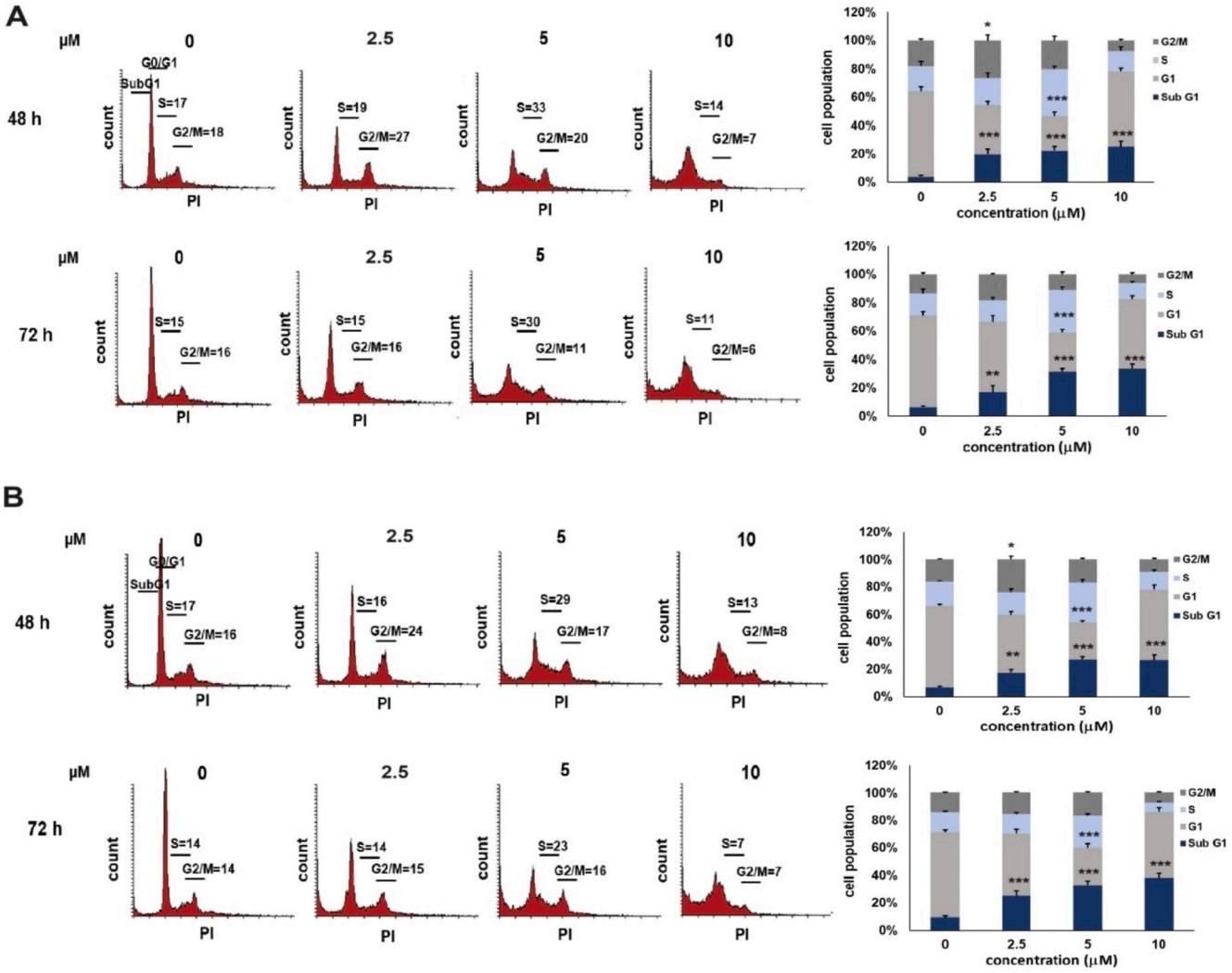

Fig. 6. Cell cycle arrest induced by compounds **9** and **19** in the G2/M and S phase in MCF-7 cells. Cells were treated with the indicated concentrations of compounds **9** (**A**) and **19** (**B**) for 48 h and 72 h, and cell cycle distribution was assessed with flow cytometry. Values are the mean ± SD of three independent experiments. Data were analyzed by one-way ANOVA with Tukey's post hoc test, $p < 0.05$ (*), $p < 0.01$ (**), $p < 0.001$ (***).

amounting to 30 % at the highest examined concentration by both compounds (Fig. 7**C**).

2.5. Analysis of MAPK/ERK activity

The MAPK/ERK signaling pathway has been reported to play a crucial role in the regulation of numerous cellular processes, such as cell proliferation, cell cycle progression, cell survival, and cell death. To evaluate the role of the MAPK/ERK pathway in the activity of compounds **9** and **19**, changes in the levels of phosphorylated ERK1/2 were assessed. For this purpose, the AlphaScreen assay, a bead-based proximity luminescent assay, was employed. With this assay, phosphorylated ERK1/2 was examined by detecting a signal generated by a cascade of energy transfer from donor beads, followed by the capture of p-ERK1/2 between donor and acceptor beads. Donor beads were conjugated with a biotinylated peptide substrate, and acceptor beads were coated with an anti-phosphotyrosine antibody. The levels of p-ERK1/2 were normalized to total ERK levels, similarly detected with the assay. The AlphaScreen assay was performed by treating cells with compounds **9** and **19** for 24 h in the concentration range of 2.5–10 μM, and the levels of p-ERK/12 and total ERK were evaluated. Additionally, the effects of the MAPK/ERK inhibitor, U0126, were evaluated by the pre-treatment of cells with this inhibitor following cell treatment with compounds **9** and **19**. The results of the AlphaScreen assay demonstrated a concentration-mediated increase in levels of p-ERK upon compound **9** and **19** treatment, whereas the levels of total ERK remained at similar levels across the tested concentrations (Fig. 8**A**). Levels of p-ERK normalized to total ERK levels, confirmed a concentration-dependent induction of p-ERK by compounds **9** and **19** (Fig. 8**B**). Furthermore, U0126 treatment significantly reduced the p-ERK levels induced by compounds **9** and **19** in MCF-7 cells (Fig. 8**C**).

2.5.1. Apoptosis and cell cycle inhibition is associated with MAPK/ERK activation

To further examine the mechanism contributing to apoptosis and cell cycle arrest induced by the examined compounds, the influence of compounds **9** and **19**-mediated ERK activation in these processes was evaluated. For this purpose, MCF-7 cells were pre-treated with the MAPK/ERK inhibitor (U0126) for 1 h following treatment with compounds **9** and **19** with the indicated concentrations. The effects of the ERK inhibitor on cell cycle-mediated disruptions induced by compounds **9** and **19** were examined with flow cytometry after PI staining. Following pre-treatment of cells with U0126, compounds **9** and **19** were examined at the concentration of 5 μM, where an increase in the S phase of the cell cycle was observed. Cells pre-treated with the ERK inhibitor were less sensitive to the cell cycle disruptive effects of compounds **9** and

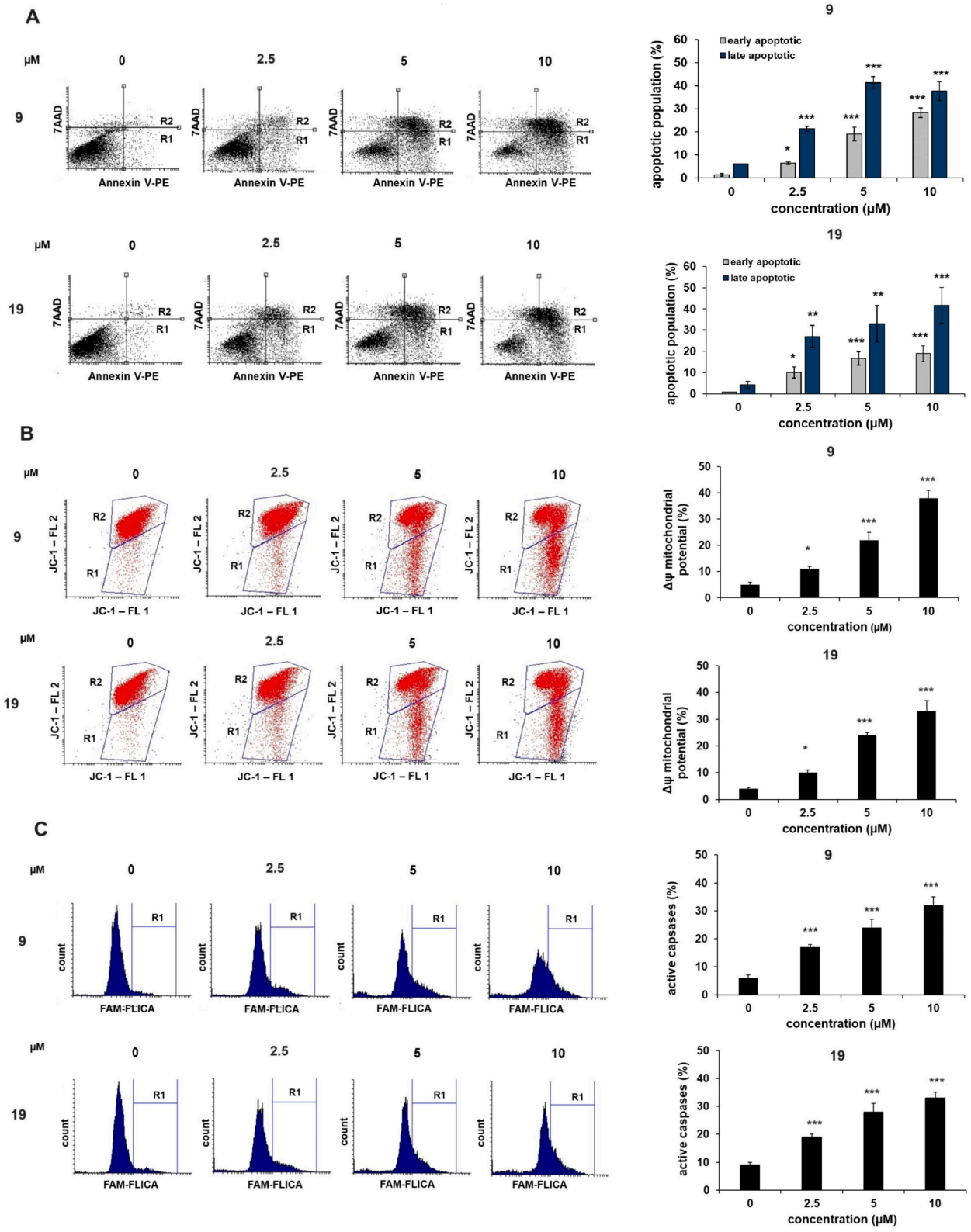

Fig. 7. Mitochondria-mediated apoptosis induction by compounds **9** and **19** in MCF-7 cells. (**A**) Induction of early and late apoptotic cell populations. Cells were treated with the indicated concentrations of compounds **9** and **19** for 72 h, stained with Annexin V-PE and 7-AAD, and assessed with flow cytometry. Dot plots and graphs show early (R1) and late (R2) apoptotic populations. (**B**) Loss of mitochondrial membrane potential (Δψm). Cells were treated with the indicated concentrations of compounds **9** and **19** for 48 h, stained with JC-1, and assessed with flow cytometry. Dot plots show JC-1 monomers (R1) and JC-1 aggregates (R2). Graphs display the increase in the release of JC-1 monomers (R1) induced by compounds **9** and **19**. (**C**) Induction of caspase activity. Cells were treated with the indicated concentrations of compounds **9** and **19** for 48 h, and caspase activity was assessed with flow cytometry with the use of a caspase inhibitor, FAM-VAD-FMK. Histograms and graphs show the increase in caspase inhibitor fluorescence (R1). Values are the mean ± SD of three independent experiments. Data were analyzed by one-way ANOVA with Tukey's post hoc test, $p < 0.05$ (*), $p < 0.01$ (**), $p < 0.001$ (***).

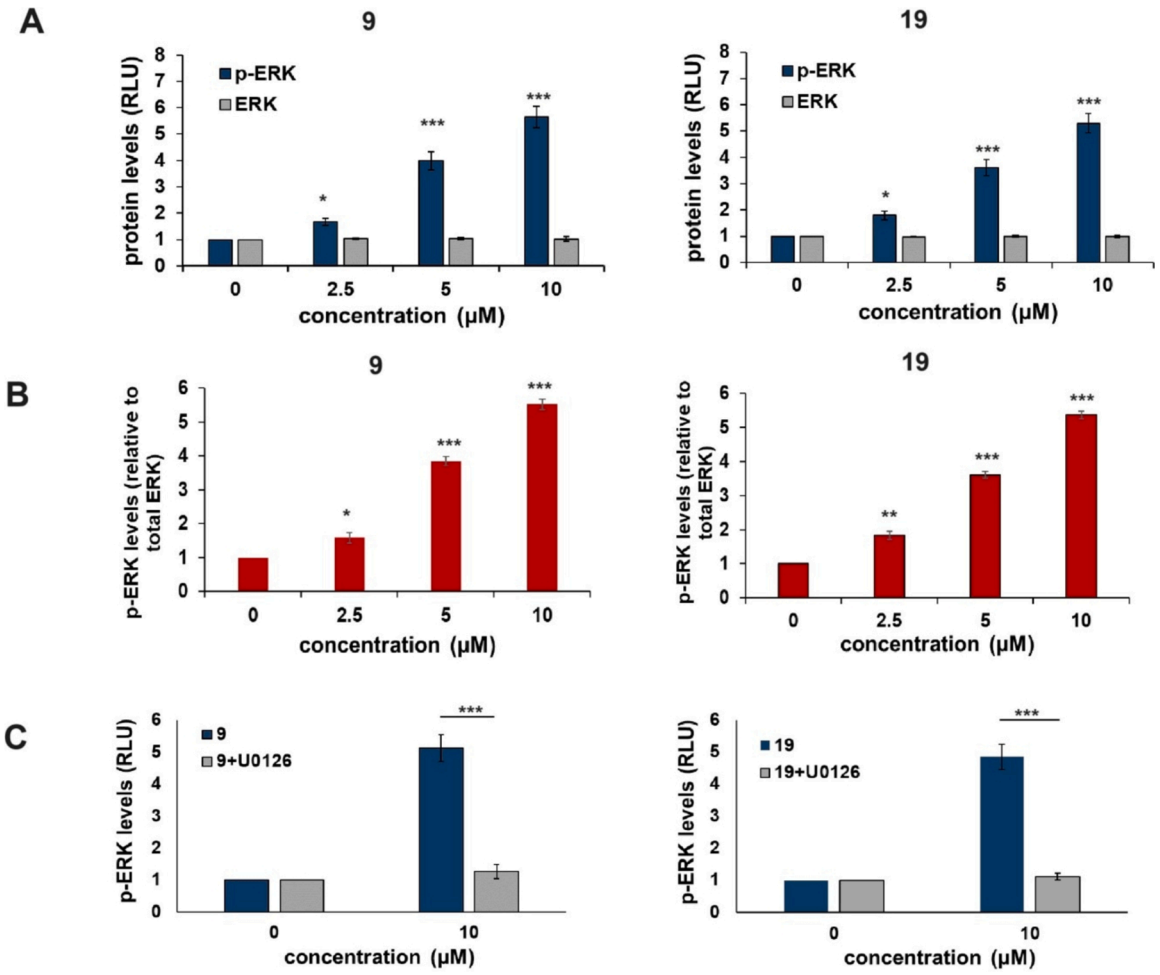

Fig. 8. Activation of MAPK/ERK by compounds **9** and **19** in MCF-7 cells. (**A**) Determination of phosphorylated ERK (p-ERK) (Thr202/Tyr204) and total ERK levels in MCF-7 cells treated with compounds **9** and **19**. (**B**) Results of p-ERK normalized to total ERK. Cells were treated with **9** and **19** for 24 h, and levels of p-ERK and ERK were determined with the AlphaScreen assay after the incubation of cell lysates with biotin-conjugated anti-p-ERK and anti-ERK antibodies and donor/acceptor beads. (**C**) Influence of the MAPK/ERK inhibitor (U0126) on compounds **9** and **19**-mediated p-ERK induction in MCF-7 cells. Cells were pre-treated with 1 μM of U0126 for 1 h, followed by a 24 h incubation of cells with 10 μM of compounds **9** and **19**. Levels of p-ERK were determined with the AlphaScreen assay. Values are the mean ± SD of three independent experiments. Data were analyzed by one-way ANOVA with Tukey's post hoc test, $p < 0.05$ (*), $p < 0.01$ (**), $p < 0.001$ (***).

19, decreasing the percentage of cells in the S phase of the cell cycle. The reduction in this population of cells was observed in the case of both compounds and reached basal control levels (Fig. 9**A**). To further verify the effects of MAPK/ERK inhibition on the pro-apoptotic activity of compounds **9** and **19**, flow cytometry analysis with Annexin V staining was used. For this purpose, following pre-treatment of cells with the ERK inhibitor, compounds **9** and **19** were examined at the concentration of 10 μM, which induced the highest increase in the apoptotic cell population. The analysis showed that the use of U0126 significantly decreased the percentage of apoptotic cells induced by both examined compounds. The apoptotic population decreased 2-fold and 2.2-fold in the case of compounds **9** and **19**, respectively (Fig. 9**B**). Collectively, these results point to the involvement of ERK pathway activation in apoptosis and the effects on cell cycle arrest mediated by compounds **9** and **19**.

3. Discussion

Benzenesulfonamides offer a promising anticancer therapeutic strategy due to the diverse mechanisms of action of these compounds. The benzenesulfonamide derivatives examined in our research induced a time and concentration-dependent transition from cell cycle arrest at the G2/M and S phases to apoptosis. Likewise, similar effects were observed in the antiproliferative activity of other benzenesulfonamide derivatives.[31] The transition from cell cycle arrest to apoptosis involves the integration of various factors and pathways, and is critical for managing the proliferation of damaged cells, an important factor in anticancer therapy. Regulation of the S and G2/M cell cycle checkpoints involves the interplay of various proteins that respond to cellular insults and changes in DNA integrity. Irreparable cellular damage as a consequence of stressor intensity and prolonged cell cycle arrest can lead to the switch from cell cycle arrest to apoptosis.[32,33] Various stress-inducible molecules or pathways, such as the tumor suppressor p53 or the MAPK pathway, modulate these signals to induce apoptosis.[33] This is associated with the influence on the expression of the Bcl-2 family proteins, which are regulators of the permeability of the mitochondrial membrane. The coordination of these proteins at the mitochondrial membrane leads to the induced activity of the pore-forming proteins (Bak/Bak), their conformational changes, oligomerization, subsequent pore-formation in the outer mitochondrial membrane, and initiation of the intrinsic apoptotic pathway.[34]

The benzenesulfonamide derivatives analyzed in our study induced apoptosis associated with the intrinsic, mitochondria-associated pathway. Various cytotoxic and proapoptotic stimuli converge on the mitochondria to facilitate the activation of mitochondria-mediated cell death. Specifically, numerous chemotherapeutic agents induce

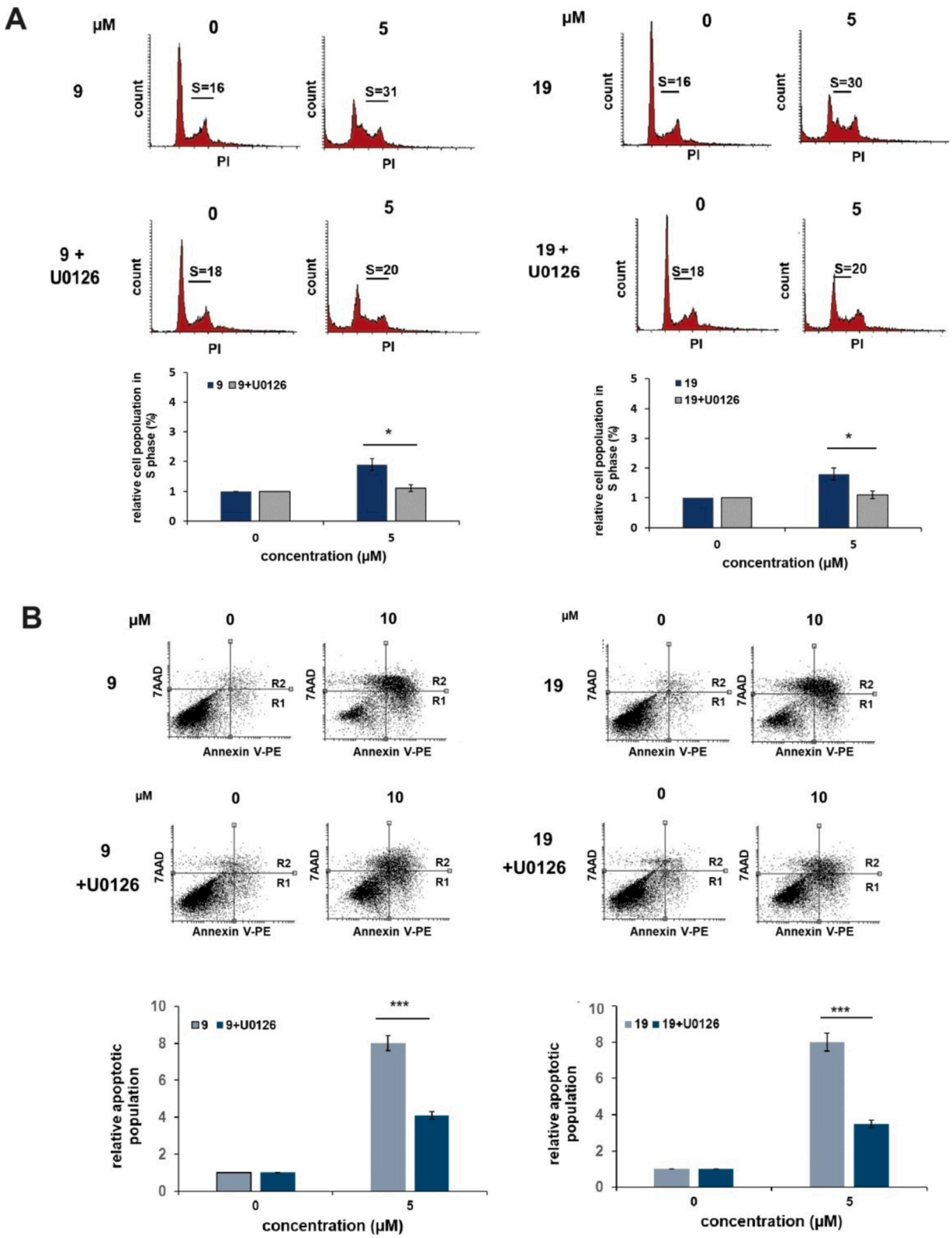

Fig. 9. MAPK/ERK-mediated cell cycle arrest and apoptosis induction by compounds **9** and **19** in MCF-7 cells. (**A**) The influence of ERK activity inhibition on compounds **9** and **19**-mediated S phase cell cycle arrest. Cells were pre-treated with U0126 (1 μM) for 1 h followed by the treatment of cells with 5 μM of compounds **9** and **19** for 48 h. Cell cycle distribution was analyzed with flow cytometry following PI staining. (**B**) The influence of ERK activity inhibition on compounds **9** and **19**-mediated apoptosis induction. Cells were pre-treated with U0126 (1 μM) for 1 h followed by the treatment of cells with 10 μM of **9** and **19** for 72 h. Apoptosis was analyzed with flow cytometry following Annexin V-PE and 7-AAD staining. Dot plots and graphs show early (R1) and late (R2) apoptotic populations. Values are the mean ± SD of three independent experiments. Data were analyzed by one-way ANOVA with Tukey's post hoc test, $p < 0.05$ (*), $p < 0.01$ (**), $p < 0.001$ (***).

mitochondrial membrane permeabilization indirectly by initiating disruptions of the intermediate metabolism or by inducing the expression of apoptotic secondary messengers. This includes increasing p53 expression, inducing the ceramide/GD3 pathway, influencing Bcl-2 protein ratios, or affecting the redox or energy balance. These factors influence the mitochondrial membrane potential, leading to its depolarization and outer membrane permeabilization.[35] This further triggers the release of cytochrome *c* from the intermembrane space and the formation of the apoptosome in the cytosol through binding to apoptotic protease-activating factor 1 (APAF1) monomers and their oligomerization. The apoptosome activates the caspase cascade leading to apoptosis execution.[34]

The mitochondrial-mediated pathway is regulated by various mechanisms in the cell. One is associated with the MAPK/ERK pathway, a cellular signaling cascade, transducing signals from cell surface receptors through a sequence of phosphorylated proteins (including Ras, Raf, MEK, and ERK) to the nucleus. The ERK protein plays an important role in regulating cell fate through its ability to phosphorylate cytoplasmic and nuclear proteins, which participate in cell proliferation, differentiation, and cell death.[4,5] Research into the role of MAPK/ERK in cell death regulation has generally depicted the activation of this pathway in cell survival. The inhibition of this pathway has contributed to the identification and development of targeted therapeutics. Nonetheless, research has shown that ERK plays dual roles in the cell, and its activation can trigger apoptosis in different cell lines. Several chemotherapeutic agents, such as cisplatin, camptothecin, or doxorubicin, have been reported to induce apoptosis through the activation of MAPK/ERK.[36,37] In our research, the examined compounds **9** and **19** induced cell cycle arrest and apoptosis in MCF-7 cells through ERK activation. This was demonstrated by the decreased sensitivity of MCF-7 cells to the activity of the benzenesulfonamides with the use of the MEK inhibitor U0126. The inhibition of ERK activity with this inhibitor decreased the percentage of the apoptotic population of cells upon benzenesulfonamide treatment. Similarly, ERK activity inhibition reduced the population of cells in the S phase of the cell cycle, collectively pointing to the ERK-mediated anti-proliferative activity of benzenesulfonamide derivatives.

The role of MAPK/ERK in mediating cell death or cell survival depends upon the kinetics of ERK activation and the intensity and duration of the stimuli. Cell death is triggered upon sustained ERK activation, whereas transient ERK stimulation results in the protection of cells against cell death.[36] In line with these findings, we observed a concentration-dependent increase in p-ERK activation, and a sustained induction of its activation, demonstrated after 24 h of incubation. Furthermore, low concentrations of the benzenesulfonamide derivatives acted through cell cycle arrest at the G2/M ad S phase, whereas higher concentrations predominately induced apoptosis. The activation of the MAPK/ERK pathway by benzenesulfonamide derivatives has been previously reported and has shown increased phosphorylation of ERK1/2 upon treatment with these compounds.[38] Our research further showed the involvement of benzenesulfonamide-mediated ERK activation in mitochondrial-induced apoptosis and cell cycle inhibition.

4. Conclusions

A series of novel 4-alkylthio-2-chloro-5-[(2-arylmethylidene)hydrazinecarbonyl]benzenesulfonamide derivatives was synthesized, using 5-(hydrazinecarbonyl)benzenesulfonamides and appropriate aldehydes. The molecular structures of novel compounds were confirmed by NMR, IR, and X-ray crystallographic analysis. The evaluation of compounds **3**–**22** against human carbonic anhydrase isozymes hCA I, hCA II, hCA IX, and hCA XII demonstrated varying degrees of activity against the studied isoenzymes. Results underscore the importance of substituent selection in designing potent inhibitors. The data reveal that the cytosolic isozyme hCA I had the lowest affinity for the tested compounds, with only compounds **18** and **20** showing significant inhibition. In contrast, the majority of 4-benzylthio-2-chloro-5-[(2-arylmethylidene)-hydrazinecarbonyl]benzenesulfonamides effectively inhibited hCA II, particularly when the phenyl group was present in the R^1 substituent, as exemplified by compound **4**. For the tumor-associated isozyme hCA IX, compounds with R^1 = Ph and R^2 = 4-ClPh or 2-OH-4-OHPh exhibited the highest inhibitory activity, with compound **3** standing out for its potency. A similar trend was observed for hCA XII inhibition, where compound **12** showed the highest activity. Research findings highlight the potential of compounds **3** and **10** as promising leads for further development, particularly against hCA IX. Compounds **9** and **10** also show strong inhibition profiles with low average K_I values, indicating their suitability for further research. Antiproliferative activity studies were carried out on three cancer cell lines – HCT-116 (colon cancer), HeLa (cervical cancer), MCF-7 (breast cancer), and a control human keratinocyte cell line, HaCaT. The obtained compounds showed the highest overall antiproliferative activity against HCT-116 cells. The most promising compounds, **9** and **19**, showed the highest cytotoxic activity toward MCF-7 cells (**9**, IC_{50} = 4 μM; **19**, IC_{50} = 6 μM) and displayed high selectivity indices for these cells (**9**, SI=8.2; **19**, SI=5.5). The antiproliferative activity of these compounds was correlated with cell cycle arrest in the G2/M and S phases at lower concentrations. Higher concentrations induced mitochondria-mediated apoptosis. The benzenesulfonamide derivatives activated the MAPK/ERK pathway, and this activity was involved in compound **9** and **19**-mediated cell cycle arrest and apoptosis. Overall, these findings underscore the potential of benzenesulfonamide derivatives as promising candidates for further research in developing novel anticancer agents with enhanced activity and selectivity.

5. Experimental

5.1. Synthesis

Melting points were uncorrected and measured using Boethius PHMK apparatus. IR spectra were measured on Thermo Mattson Satellite FTIR spectrometer in KBr pellets; an absorption range was 400–4000 cm^{-1}. ^1H NMR and ^{13}C NMR spectra were recorded on a Varian Gemini 200 apparatus or Varian Unity Plus 500 apparatus. Chemical shifts are expressed at δ values relative to Me_4Si (TMS) as an internal standard. The apparent resonance multiplicity is described as: s (singlet), d (doublet), dd (doublet of doublets), t (triplet), m (multiplet), and br (broad) signal. Elemental analyses were performed on PerkinElmer 2400 Series II CHN Elemental Analyzer and the results were within ±0.4 % of the theoretical values. Thin-layer chromatography (TLC) was performed on Merck Kieselgel 60 F254 plates and visualized with UV. Mobile phases for TLC: A – benzene: ethanol (4:1 v/v); B – chloroform: methanol (16:3 v/v); C – chloroform: methanol (16:1 v/v). Purity of compounds was analyzed by RP-HPLC on Shimadzu (Model LC-10AD) HPLC system; Column: Gemini 4.6 × 250 mm; C6-phenyl; 5 μm; 110 Å, Mobile Phase: A – grade water with 0.1 % (v/v) trifluoroacetic acid, B – 80 % acetonitrile–water containing 0.08 % (v/v) trifluoroacetic acid, linear gradient 0–100 % B in 30 min, Flow Rate: 1 ml/min. The purity of compounds was >95 %, as determined by RP-HPLC. The MALDI TOFTOF 5800 Sciex spectrometer was used to analyze obtained compounds. Samples were dissolved in methanol with 5 % water content, and ferulic acid (FA, concentration 10 mg/mL in 33 % acetonitrile/17 % formic acid in water) was used as the matrix. Supplementary material contains NMR, MS spectra, HPLC chromatograms, and elemental analyses.

5.1.1. 4-Benzylthio-2-chloro-5-(hydrazinecarbonyl)benzenesulfonamide (1)

To a suspension of 2,4-dichloro-5-sulfoamoylbenzohydrazide (4.27 g, 15 mmol), K_2CO_3 (4.15 g, 31 mmol), TBAI (0.05 g, 0.15 mmol) in 50 mL MeCN and 0.5 mL water, benzylthiol (1.86 g, 15 mmol) was added dropwise under argon. The reaction mixture was stirred at room

temperature for 24 h. After reaction the mixture was concentrated to dryness under reduced pressure, 100 mL of 0.5 M HCl was added, and then pH was adjusted to 6–7 with 10 % aqueous K_2CO_3 solution. The crude product was filtered off, washed with a 10 % aqueous K_2CO_3 and water. A pure compound was obtained after crystallization from ethanol. Yield 2.729 g (49 %) of the title compound **1**: m.p. 210–215 °C; R_f = 0.67 (B). IR (KBr) 3362, 3320 (N—H); 3063 (CAr-H); 2925, 2851 (CH_3); 1670 (N—H); 1574 (C═N); 1527 (C═C); 1325 (SO_2 *asym*); 1162 (SO_2 *sym*) cm^{-1}; ^{1}H NMR (500 MHz, 100 °C, DMSO-d_6): δ 4.31 [s, 2H, CH_2-S]; 4.46 [s, 2H, NH_2]; 7.25 [t, $^3J_{HH}$=7.8 Hz, 1H, arom]; 7.28 [s, 2H, SO_2NH_2]; 7.32 [t, $^3J_{HH}$ = 7.8 Hz, 7.3 Hz, 2H, arom]; 7.39 [d, $^3J_{HH}$ = 7.3 Hz, 2H, arom]; 7.55 [s, 1H, H-3]; 7.87 [s, 1H, H-6]; 9.43 [s,1H, NH] ppm.

5.1.2. 2-Chloro-4-[(4-fluorophenyl)methylthio]-5-(hydrazinecarbonyl) benzenesulfonamide (2)

To a suspension of 2,4-dichloro-5-sulfoamoylbenzohydrazide (1.4 g, 4.93 mmol), K_2CO_3 (1.41 g, 10.18 mmol), TBAI (0.018 g, 0.05 mmol) in 16 mL MeCN and 0.16 mL water, (4-fluorophenyl)methanethiol (1.86 g, 15 mmol) was added dropwise under argon. The reaction mixture was stirred at room temperature for 95 h. After reaction the mixture was concentrated to dryness under reduced pressure, 100 mL of 0.5 M HCl was added, and then pH was adjusted to 6–7 with 10 % aqueous K_2CO_3 solution. The crude product was filtered off, washed with a 10 % aqueous K_2CO_3, water and dry an infrared lamp. A pure compound was obtained after crystallization from ethanol. Yield 0.900 g (47 %) of the title compound **2**: m.p. 168–170 °C; R_f = 0.47 (A), R_f = 0.62 (B). IR (KBr) 3331, 3269 (N—H); 3073, 3042 (C_{Ar}-H); 2971, 2926 (CH_3); 1647 (N—H); 1575 (C═N); 1508 (C═C); 1332 (SO_2 *asym*); 1163 (SO_2 *sym*) cm^{-1}; ^{1}H NMR (500 MHz, 100 °C, DMSO-d_6): δ 4.33 [s, 2H, CH_2-S]; 4.42 [s, 2H, NH_2]; 7.13 [dd, $^3J_{HH}$=8 Hz, 2H, arom]; 7.32 [s, 2H, SO_2NH_2]; 7.44 [dd, $^3J_{HH}$=8 Hz, 2H, arom]; 7.57 [s, 1H, H-3]; 7.90 [s, 1H, H-6]; 9.46 [s, 1H, NH] ppm. HRMS (MALDI-TOF/TOF) *m/z* calculated for $[M+H]^+$ = 389.8527, found $[M+H]^+$ = 389.9641.

5.1.3. Synthesis procedure for final 4-benzylthio-2-chloro-5-[(2-arylmethylidene)-hydrazinecarbonyl]benzenesulfonamides 3–12

The mixture of **1** (200 mg, 0.538 mmol) and an appropriate aldehyde (0.565 mmol) in ethanol (5 mL) with the addition of one drop of sulfuric (VI) acid was stirred at 90 °C for 0.5–2.5 h. The progress of the reaction was monitored by TLC. After the reaction, the reaction mixture was left in the refrigerator for 6 h. The resulting precipitate was filtered off, dried under an infrared lamp, and then in a vacuum oven at 110 °C for 24 h. If necessary, the recrystallization from ethanol was applied.

5.1.3.1. 4-Benzylthio-2-chloro-5-[2-(4-chlorobenzylidene)hydrazinecarbonyl]benzenesulfonamide (3).

Starting with **1** (200 mg) and 4-chlorobenzaldehyde (80 mg) for 30 min, the title compound **3** was obtained (243 mg, 92 %): m.p. 254–255 °C; HPLC t_R = 28.94 min; R_f = 0.88 (A), R_f = 0.84 (B), R_f = 0.5 (C); IR (KBr) 3427, 3214 (N—H); 3065 (C_{Ar}-H); 2920 (CH_3); 1642 (N—H); 1591 (C═N); 1494 (C═C); 1354, 1171 (SO_2) cm^{-1}; ^{1}H NMR (500 MHz, DMSO-d_6): δ 4.40 [s, 2H, CH_2-S]; 7.06–7.94 [m, 12H, arom, NH]; 8.00 [s, 1H, arom]; 8.30 [s, 1H, N = CH]; 12.13 [s, 1H, NH] ppm. HRMS (MALDI-TOF/TOF) *m/z* calculated for $[M + H]^+$ = 494.0167, found $[M + H]^+$ = 493.9873.

5.1.3.2. 4-Benzylthio-5-[2-(4-bromobenzylidene)hydrazinocarbonyl]-2-chlorobenzenesulfonamide (4).

Starting with **1** (200 mg) and 4-bromobenzaldehyde (105 mg) for 45 min, the title compound **4** was obtained after recrystallization from ethanol (241 mg, 83 %): m.p. 260–261 °C; HPLC t_R = 28.71 min; R_f = 0.7 (A), R_f = 0.42 (C). IR (KBr): 3428, 3215 (N—H); 3065 (C_{Ar}-H); 2917 (CH_3); 1643 (N—H); 1549 (C═N); 1494 (C═C); 1354 (SO_2 *asym*); 1171 (SO_2 *sym*) cm^{-1}; ^{1}H NMR (500 MHz, DMSO-d_6): δ 4.40 [s, 2H, CH_2-S]; 7.27 [t, 1H, arom]; 7.34 [t, 2H, arom]; 7.42 [d, $^3J_{HH}$ = 7.3 Hz, 2H, arom]; 7.58 [d, $^3J_{HH}$ = 7.8 Hz, 2H, arom]; 7.65 [brs, 2H, NH_2]; 7.67 [s, 1H, H-3]; 7.72 [d, 2H, arom]; 8.02 [s, 1H, H-6]; 8.29 [s, 1H, N=CH]; 12.10 [s, 1H, NH] ppm. HRMS (MALDI-TOF/TOF) *m/z* calculated for $[M+H]^+$ = 537.9661, found $[M + H]^+$ = 537.9240.

5.1.3.3. 4-Benzylthio-2-chloro-5-[2-(4-fluorobenzylidene)hydrazinecarbonyl]benzenesulfonamide (5).

Starting with **1** (200 mg) and 4-fluorobenzaldehyde (70 mg) for 50 min, the title compound **5** was obtained (216 mg, 84 %): m.p. 247–248 °C; HPLC t_R=27.28 min; R_f = 0.46 (C). IR (KBr) 3380, 3208 (N—H); 3064 (C_{Ar}-H); 1635 (N—H); 1553 (C═N); 1507 (C═C); 1352 (SO_2 *asym*); 1174, 1154 (SO_2 *sym*) cm^{-1}; ^{1}H NMR (500 MHz, DMSO-d_6): δ 4.41 [s, 2H, CH_2-S]; 7.08–7.37 [m, 5H, arom]; 7.42 [d, $^3J_{HH}$=7.3 Hz, 2H, arom]; 7.68 [d, $^3J_{HH}$ = 7.8 Hz, 2H, arom]; 7.73 [brs, 2H, NH_2]; 7.80 [dd, $^3J_{HH}$ = 8.3 Hz, 2H, arom]; 8.03 [s, 1H, H-6]; 8.30 [s, 1H, N = CH]; 12.08 [s, 1H, NH] ppm. HRMS (MALDI-TOF/TOF) *m/z* calculated for $[M + H]^+$ = 478.0462, found $[M + H]^+$ = 477.9991.

5.1.3.4. 4-Benzylthio-2-chloro-5-[2-(benzylidenehydrazinecarbonyl]benzenesulfonamide (6).

Starting with **1** (200 mg) and benzaldehyde (60 mg) for 1 h, the title compound **6** was obtained (193 mg, 78 %): m.p. 226–228 °C; HPLC t_R=26.95 min; R_f = 0.5 (C). IR (KBr) 3416, 3338, 3210 (N—H); 3059 (C_{Ar}-H); 2925, 2852 (CH_3); 1634 (N—H); 1552 (C═N); 1494 (C═C); 1352 (SO_2 *asym*); 1175 (SO_2 *sym*) cm^{-1}; ^{1}H NMR (500 MHz, 100 °C, DMSO-d_6): δ 4.34 [s, 2H, CH_2-S]; 7.22 [t, 1H, arom]; 7.28 [t, 2H, arom]; 7.32–7.38 [m, 4H, arom]; 7.39–7.46 [m, 3H, arom]; 7.60 [brs, 2H, NH_2]; 7.64 [s, 1H, H-3]; 7.96 [s, 1H, H-6]; 8.24 [s, 1H, N = CH]; 11.68 [s, 1H, NH] ppm. HRMS (MALDI-TOF/TOF) *m/z* calculated for $[M + H]^+$ = 460.0556, found $[M + H]^+$ = 460.0804.

5.1.3.5. 4-Benzylthio-2-chloro-5-[2-(4-nitrobenzylidene)hydrazinecarbonyl]benzenesulfonamide (7).

Starting with **1** (200 mg) and 4-nitrobenzaldehyde (85 mg) for 1 h, the title compound **7** was obtained after recrystallization from ethanol (272 mg, 79 %): m.p. 271–272 °C; HPLC t_R=27.97 min; R_f = 0.53 (C). IR (KBr) 3415, 3221 (N—H); 3063 (C_{Ar}-H); 2927, 2850 (CH_3); 1648 (N—H); 1572 (C═N); 1510 (C═C); 1343 (SO_2 *asym*); 1173 (SO_2 *sym*) cm^{-1}; ^{1}H NMR (500 MHz, DMSO-d_6): δ 4.42 [s, 2H, CH_2-S]; 7.27 [t, 1H, arom]; 7.34 [t, 2H, arom]; 7.42 [d, 2H, arom]; 7.66 [brs, 2H, NH_2]; 7.68 [s, 1H, H-3]; 7.73–7.99 [m, 2H, arom]; 8.01 [s, 1H, H-6]; 8.12–8.37 [m, 2H, arom]; 8.42 [s, 1H, N = CH]; 12.34 [s, 1H, NH] ppm. HRMS (MALDI-TOF/TOF) *m/z* calculated for $[M(NO_2) + H]^+$ = 505.0407, found $[M(NH_2) + H]^+$ = 475.0240 (the found mass corresponds to the mass of the ion where nitro group under ionization conditions has been reduced to the amino group, which corresponds to the calculated sum formula $C_{21}H_{19}ClN_4O_3S_2$ and $[M(NH_2) + H]^+$ = 475.0665).

5.1.3.6. 4-Benzylthio-2-chloro-5-[2-(4-trifluoromethylbenzylidene)hydrazinecarbonyl]benzenesulfonamide (8).

Starting with **1** (200 mg) and 4-trifluorobenzaldehyde (93 mg) for 1 h, the title compound **8** was obtained (193 mg, 68 %): m.p. 253–255 °C; HPLC t_R=28.96 min; R_f = 0.52 (C). IR (KBr) 3383, 3216 (N—H); 3066 (C_{Ar}-H); 2931, 2854 (CH_3); 1642 (N—H); 1574 (C═N); 1496 (C═C); 1348, 1325 (SO_2 *asym*); 1170 (SO_2 *sym*) cm^{-1}; ^{1}H NMR (500 MHz, DMSO-d_6): δ 4.43 [s, 2H, CH_2-S]; 7.15–7.30 [m, 3H, arom]; 7.43 [d, 2H, arom]; 7.68 [brs, 2H, NH_2]; 7.70 [s, 1H, H-3]; 7.72–7.79 [m, 2H, arom]; 7.90 [dd, $^3J_{HH}$ = 7.8 Hz, 2H, arom]; 8.15 [s, 1H, H-6]; 8.38 [s, 1H, N = CH]; 12.26 [s, 1H, NH] ppm. HRMS (MALDI-TOF/TOF) *m/z* calculated for $[M + H]^+$ = 528.0430, found $[M + H]^+$ = 528.0266.

5.1.3.7. 4-Benzylthio-5-[2-(4-bromo-2-hydroxybenzylidene)hydrazinecarbonyl]-2-chlorobenzenesulfonamide (9).

Starting with **1** (200 mg) and 4-bromosalicylaldehyde (114 mg) for 1 h, the title compound **9** was obtained (278 mg, 93 %): m.p. 271–272 °C; HPLC t_R=29.43 min; R_f = 0.78 (A) R_f = 0.20 (C); IR (KBr) 3331 (O—H); 3262, 3213 (N—H); 3059 (C_{Ar}-H); 2853 (CH_3); 1642 (N—H); 1574 (C═N); 1494 (C═C); 1354

(SO_2 *asym*); 1171 (SO_2 *sym*) cm^{-1}; ^1H NMR (500 MHz, DMSO-d_6): δ 4.42 [s, 2H, CH_2-S]; 6.93–7.30 [m, 3H, arom,]; 7.34 [t, 2H, arom]; 7.43 [d, $^3J_{HH}$ = 7.3 Hz, 1H, arom]; 7.59 [d, $^3J_{HH}$ = 8.3 Hz, 1H arom]; 7.67 [brs, 2H, NH_2]; 7.73 [s, 1H H-3]; 8.02 [s, 1H, H-6]; 8.51 [s, 1H, arom]; 11.24 [s, 1H, OH]; 12.28 [s, 1H, NH] ppm; ^{13}C NMR (125 MHz, 140 °C, DMSO-d_6): δ 37.8, 119.2, 119.8, 123.0, 124.5, 127.7, 128.8, 128.9, 129.2, 129.8, 130.8, 132.6, 136.7, 138.7, 142.6, 153.1, 158.5 ppm. HRMS (MALDI-TOF/TOF) *m/z* calculated for $[M + H]^+$ = 553.9610, found $[M + H]^+$ = 553.8870.

5.1.3.8. 4-Benzylthio-2-chloro-5-[2-(2,4-dihydroxybenzylidene)hydrazinecarbonyl]benzenesulfonamide (10). Starting with **1** (200 mg) and 2,4-dihydroxybenzaldehyde (78 mg) for 1 h, the title compound **10** was obtained (101 mg, 38 %): m.p. 149–151 °C; HPLC t_R=25.01 min; R_f = 0.72 (A). IR (KBr) 3373, 3237 (N—H); 3084 (C_{Ar}-H); 1630 (N—H); 1578 (C═N); 1513 (C═C); 1344 (SO_2 *asym*); 1170 (SO_2 *sym*) cm^{-1}; ^1H NMR (500 MHz, DMSO-d_6): δ 4.41 [s, 2H, CH_2-S]; 6.15–6.47 [m, 2H]; 7.27 [t, 1H, arom]; 7.34 [t, 2H, arom]; 7.43 [d, 2H, arom]; 7.64 [brs, 2H, NH_2]; 7.66 s, 1H, arom]; 7.71 [s, 1H, H-3]; 8.00 [s, 1H, H-6]; 8.39 [s, 1H, N=CH]; 9.97 [s, 1H, OH]; 11.15 [s, 1H, OH]; 12.04 [s, 1H, NH] ppm. HRMS (MALDI-TOF/TOF) *m/z* calculated for $[M+H]^+$ = 492.0455, found $[M+H]^+$ = 492.0024.

5.1.3.9. 4-Benzylthio-5-[2-(quinolin-2-ylmethylene)hydrazinocarbonyl]-2-chlorobenzenesulfonamide (11). Starting with **1** (200 mg) and 2-quinolinecarboxaldehyde (89 mg) for 2.5 h, the title compound **11** was obtained after recrystallization from ethanol (191 mg, 70 %): m.p. 247–248 °C; HPLC t_R=23.53 min; R_f = 0.84 (A); IR (KBr) 3349, 3202 (N—H); 3076 (C_{Ar}-H); 1674 (N—H); 1576 (C═N); 1495 (C═C); 1347 (SO_2 *asym*); 1172 (SO_2 *sym*) cm^{-1}; ^1H NMR (500 MHz, DMSO-d_6): δ 4.44 [s, 2H, CH_2-S]; 7.14–7.51 [m, 5H, arom]; 7.68 [s, 3H, H-3, NH_2]; 7.77 [s, 1H, arom]; 7.83 [t, 1H, arom]; 7.91–8.10 [m, 3H, arom]; 8.13 [d, 1H, arom]; 8.31 [d, 1H, arom]; 8.48 [s, 1H, N = CH]; 12.44 [s, 1H, NH] ppm. HRMS (MALDI-TOF/TOF) *m/z* calculated for $[M + H]^+$ = 511.0665, found $[M + H]^+$ = 511.0384.

5.1.3.10. 4-Benzylthio-2-chloro-5-[2-(pyridin-4-ylmethylene)hydrazinecarbonyl]benzenesulfonamide (12). Starting with **1** (200 mg) and 4-pyridine carboxaldehyde (61 mg) for 2 h, the title compound **12** was obtained (260 mg, 92 %): m.p. 185–186 °C; HPLC t_R=18.27 min; R_f = 0.68 (A), R_f = 0.65 (B). IR (KBr) 3315, 3147 (N—H); 3055 (C_{Ar}-H); 2855, 2777 (CH_3); 1637 (N—H); 1584 (C═N); 1505 (C═C); 1310 (SO_2 *asym*); 1172 (SO_2 *sym*) cm^{-1}; ^1H NMR (500 MHz, DMSO-d_6): δ 4.39 [s, 2H, CH_2-S]; 7.24 [t, 1H, arom]; 7.30 [t, 2H, arom]; 7.38 [d, 2H, arom]; 7.50 [d, 2H, pyridyl]; 7.72 [s, 1H, H-3]; 7.86 [brs, 2H, NH_2]; 8.01 [s, 1H, H-6]; 8.35 [s, 1H, N = CH]; 8.77 [d, 2H, pyridyl]; 12.37 [s, 1H, NH] ppm; ^{13}C NMR (125 MHz, 140 °C, DMSO-d_6): δ 37.9, 122.6, 127.8, 128.9, 128.9, 129.2, 131.0, 132.6, 134.3, 136.8, 138.8, 142.5, 143.9, 145.8, 147.2, 151.1 ppm. HRMS (MALDI-TOF/TOF) *m/z* calculated for $[M + H]^+$ = 461.0509, found $[M + H]^+$ = 461.0315.

5.1.4. Synthesis procedure for final 2-chloro-4-[(4-fluorophenyl)methylthio]-5-(hydrazinecarbonyl)benzenesulfonamide 13–22

The mixture of **2** (90 mg, 0.231 mmol) and an appropriate aldehyde (0.242 mmol) in ethanol (2.5 mL) with the addition of one drop of sulfuric(VI) acid was stirred at 90 °C for 45 min–2.5 h. The progress of the reaction was monitored by TLC. After the reaction, the reaction mixture was left in the fridge for 1 h. The resulting precipitate was filtered off, dried under an infrared lamp, and then in a vacuum oven at 110 °C for 24 h. If necessary, the recrystallization from ethanol and/or acetonitrile was applied.

5.1.4.1. 2-Chloro-5-[2-(4-chlorobenzylidene)hydrazinecarbonyl]-4-[(4-fluorophenyl)methylthio]benzenesulfonamide (13). Starting with **2** (90 mg) and 4-chlorobenzaldehyde (34 mg) for 45 min, the title compound **13** was obtained after recrystallization from ethanol/acetonitrile mixture (v/v = 1/1) (74 mg, 63 %): m.p. 276–277 °C; HPLC t_R = 28.54 min; R_f = 0.80 (A), R_f = 0.50 (C). IR (KBr) 3433, 3227 (N—H); 3066 (C_{Ar}-H); 2955, 2928, 2853 (CH_3); 1648 (N—H); 1573 (C═N); 1510 (C═C); 1354 (SO_2 *asym*); 1171 (SO_2 *sym*) cm^{-1}; ^1H NMR (500 MHz, DMSO-d_6, 100 °C): δ 4.36 [s, 2H, CH_2-S]; 7.08 [dd, $^3J_{HH}$ = 8 Hz, 2H, arom]; 7.25–7.50 [m, 6H, arom]; 7.62 [brs, 2H, NH_2]; 7.67 [s, 1H, H-3]; 7.98 [s, 1H, H-6]; 8.25 [s,1H, N = CH]; 11.77 [s, 1H, NH] ppm. HRMS (MALDI-TOF/TOF) *m/z* calculated for $[M + H]^+$ = 512.0072, found $[M + H]^+$ = 511.9908.

5.1.4.2. 5-[2-(4-Bromobenzylidene)hydrazinecarbonyl]-2-chloro-4-(4-fluorobenzylthio)benzenesulfonamide (14). Starting with **2** (90 mg) and 4-bromobenzaldehyde (45 mg) for 45 min, the title compound **14** was obtained after recrystallization from acetonitrile (78 mg, 61 %): m.p. 270–271 °C; HPLC t_R = 31.84 min; R_f = 0.74 (A), R_f = 0.44 (C). IR (KBr) 3435, 3231 (N—H); 3067 (C_{Ar}-H); 2974, 2928, 2896, 2855 (CH_3); 1648 (N—H); 1571 (C═N); 1511 (C═C); 1354 (SO_2 *asym*); 1171 (SO_2 *sym*) cm^{-1}; ^1H NMR (500 MHz, DMSO-d_6, 100 °C): δ 4.36 [s, 2H, CH_2-S]; 7.08 [dd, $^3J_{HH}$ = 8 Hz, 2H, arom]; 7.25–7.45 [m, 4H, arom]; 7.50–7.65 [m, 4H, arom, NH]; 7.66 [s, 1H, H-3]; 7.98 [s, 1H, H-6]; 8.23 [s, 1H, N = CH]; 11.77 [s, 1H, NH] ppm. HRMS (MALDI-TOF/TOF) *m/z* calculated for $[M + H]^+$ = 555.9567, found $[M + H]^+$ = 555.9124.

5.1.4.3. 2-Chloro-5-[2-(4-fluorobenzylidene)hydrazinecarbonyl]-4-[(4-fluorophenyl)methylthio]benzenesulfonamide (15). Starting with **2** (90 mg) and 4-fluorobenzaldehyde (30 mg) for 45 min, the title compound **15** was obtained (85 mg, 74 %): m.p. 254–255 °C; HPLC t_R = 30.43 min; R_f = 0.73 (A), R_f = 0.28 (C). IR (KBr) 3411, 3267, 3234 (N—H); 3070 C_{Ar}-H); 2933, 2858, 2799 (CH_3); 1643 (N—H);1577 (C═N); 1509 (C═C); 1348 (SO_2 *asym*); 1172 (SO_2 *sym*) cm^{-1}; ^1H NMR (500 MHz, DMSO-d_6, 100 °C): δ 4.36 [s, 2H, CH_2-S]; 7.08 [dd, $^3J_{HH}$=8 Hz, 2H, arom]; 7.23 [dd, $^3J_{HH}$=8 Hz, 2H, arom]; 7.30–7.50 [m, 4H, arom]; 7.51–7.86 [m, 3H, arom, NH_2]; 7.97 [s, 1H, H-6]; 8.26 [s, 1H, N = CH]; 11.71 [s, 1H, NH] ppm; ^{13}C NMR (125 MHz, 140 °C, DMSO-d_6): δ 37.1, 115.5, 115.7, 116.0, 116.2, 128.9, 129.6, 129.7, 131.1, 131.2, 131.3, 132.2, 133.1, 138.8, 161.1, 162.8, 163.1, 164.8 ppm. HRMS (MALDI-TOF/TOF) *m/z* calculated for $[M + H]^+$ = 496.0368, found $[M + H]^+$ = 496.0150.

5.1.4.4. 5-(2-Benzylidenhydrazinecarbonyl)-2-chloro-4-[(4-fluorophenyl) methylthio]benzenesulfonamide (16). Starting with **2** (90 mg) and benzaldehyde (26 mg) for 1.5 h, the title compound **16** was obtained (89 mg, 81 %): m.p. 222–223 °C; HPLC t_R=30.14 min; R_f = 0.65 (A), R_f = 0.28 (C); IR (KBr) 3341, 3246 (N—H); 3110, 3067 (C_{Ar}-H); 2970, 2922 (CH_3); 1685 (N—H); 1574 (C═N); 1507 (C═C); 1345 (SO_2 *asym*); 1180 (SO_2 *sym*) cm^{-1}; ^1H NMR (500 MHz, DMSO-d_6, 100 °C): δ 4.36 [s, 2H, CH_2-S]; 7.08 [dd, $^3J_{HH}$ = 8 Hz, 2H, arom]; 7.32–7.50 [m, 8H, arom]; 7.60 [brs, 1H, NH_2]; 7.66 [s, 1H, H-3]; 7.98 [s, 1H, H-6]; 8.26 [s, 1H, N = CH]; 11.70 [s, 1H, NH] ppm. HRMS (MALDI-TOF/TOF) *m/z* calculated for $[M + H]^+$ = 478.0462, found $[M + H]^+$ = 478.0433.

5.1.4.5. 2-Chloro-4-[(4-fluorophenyl)methylthio]-5-[2-(4-nitrobenzylidene)hydrazinecarbonyl]benzenesulfonamide (17). Starting with **2** (90 mg) and 4-nitrobenzaldehyde (37 mg) for 50 min, the title compound **17** was obtained after recrystallization from acetonitrile (71 mg, 59 %): m.p. 290–291 °C; HPLC t_R = 27.71 min; R_f = 0.67 (A), R_f = 0.83 (B). IR (KBr) 3415, 3236 (N—H); 3116, 3060 (C_{Ar}-H); 2932, 2855 (CH_3); 1648 (N—H); 1574 (C═N); 1508 (C═C); 1343 (SO_2 *asym*); 1174 (SO_2 *sym*) cm^{-1}; ^1H NMR (500 MHz, DMSO-d_6, 100 °C): δ 4.37 [s, 1H, CH_2-S]; 7.08 [dd, $^3J_{HH}$=8 Hz, 2H, arom]; 7.30–7.50 [m, 4H, arom]; 7.69 [s, 1H, H-3]; 7.85 [brs, 2H, NH_2]; 8.00 [s, 1H, H-6]; 8.24 [d, 2H, arom]; 8.36 [s, 1H, N = CH]; 12.02 [s, 1H, NH] ppm. HRMS (MALDI-TOF/TOF) *m/z* calculated for $[M(NO_2) + H]^+$ = 523.0313, found $[M(NH_2) + H]^+$ = 493.0092 (The found *m/z* corresponds to the ion with the reduced nitro

group. Under the ionization conditions during the analysis, the nitro group in compound **17** has been reduced to an amino group. This reduction corresponds to the molecular formula $C_{21}H_{19}ClN_4O_3S_2$ and [M (NH_2) + H]$^+$ = 493.0493).

5.1.4.6. 2-Chloro-4-[(4-fluorophenyl)methylthio]-5-[2-(4-trifluoromethylbenzylidene)hydrazinecarbonyl]benzenesulfonamide (18). Starting with **2** (90 mg) and 4-trifluoromethylbenzaldehyde (42 mg) for 50 min, the title compound **18** was obtained (79 mg, 63 %): m.p. 249–250 °C; HPLC t_R = 29.07 min; R_f = 0.61(A), R_f = 0.25 (C). IR (KBr) 3420, 3380, 3207 (N—H); 3074, 3047 (C_{Ar}-H); 2936, 2855 (CH_3); 1637 (N—H); 1575 (C═N); 1509 (C═C); 1325 (SO_2 *asym*); 1172 (SO_2 *sym*) cm^{-1}; ^{1}H NMR (500 MHz, DMSO-d_6, 100 °C): δ 4.35 [s, 2H, CH_2-S]; 7.08 [dd, $^3J_{HH}$ = 8 Hz, 2H, arom]; 7.30–7.50 [m, 4H, arom]; 7.68 [s, 1H, H-3]; 7.75 [d, $^3J_{HH}$ = 7 Hz, 2H, arom]; 7.80 [brs, 2H, NH_2]; 7.99 [s, 1H, H-6]; 8.32 [s, 1H, N = CH]; 11.91 [s, 1H, NH] ppm. HRMS (MALDI-TOF/TOF) *m/z* calculated for [M + H]$^+$ = 546.0336, found [M + H]$^+$ = 545.9902.

5.1.4.7. 5-[2-(4-Bromo-2-hydroxybenzylidene)hydrazinecarbonyl]-2-chloro-4-[(4-fluorophenyl)methylthio])benzenesulfonamide (19). Starting with **2** (90 mg) and 4-bromosalicylaldehyde (48 mg) for 1 h 25 min, the title compound **19** was obtained (111 mg, 84 %): M.p. 244–245 °C; HPLC t_R=29.76 min; R_f = 0.68 (A). IR (KBr) 3334, 3263, 3206, 3186 (N—H); 3052 (C_{Ar}-H); 2920, 2853 (CH_3); 1640 (N—H); 1574 (C═N); 1508 (C═C); 1342 (SO_2 *asym*); 1170 (SO_2 *sym*) cm^{-1}; ^{1}H NMR (500 MHz, DMSO-d_6, 100 °C): δ 4.37 [s, 2H, CH_2-S]; 6.93–7.20 [m, 4H, arom]; 7.30–7.62 [m, 5H, arom, NH_2]; 7.67 [s, 1H, H-3]; 8.01 [s, 1H, H-6]; 8.47 [s, 1H, N = CH]; 11.14 [brs, 1H, OH]; 11.93 [s, 1H, NH] ppm; ^{13}C NMR (125 MHz, 140 °C, DMSO-d_6): δ 37.0, 115.5, 115.7, 119.2, 119.8, 123.0, 123.2, 124.5, 128.8, 130.8, 130.8, 131.0, 131.1, 131.2, 132.9, 133.0,138.9, 153.5, 158.5 ppm. HRMS (MALDI-TOF/TOF) *m/z* calculated for [M + H]$^+$ = 571.9516, found [M + H]$^+$ = 571.9017

5.1.4.8. 2-Chloro-4-[(4-fluorophenyl)methylthio]-5-[2-(2,4-dihydroxybenzylidene)hydrazinecarbonyl]benzenesulfonamide (20). Starting with **2** (90 mg) and 2,4-dihydroxybenzaldehyde (33 mg) for 2 h, the title compound **20** was obtained after recrystallization from ethanol (61 mg, 52 %): m.p. 152–153 °C; HPLC t_R = 25.19 min; R_f = 0.50 (A), R_f = 0.61 (B). IR (KBr) 3499 (O—H); 3353, 3200 (N—H); 3078 (C_{Ar}-H); 2975, 2926, 2898 (CH_3); 1629 (N—H); 1584 (C═N); 1512 (C═C); 1346 (SO_2 *asym*); 1173 (SO_2 *sym*) cm^{-1}; ^{1}H NMR (500 MHz, DMSO-d_6, 100 °C): δ 4.37 [s, 2H, CH_2-S]; 6.16–6.50 [m, 2H]; 7.10 [dd, $^3J_{HH}$ = 7 Hz, 2H, arom]; 7.25 [s, 1H]; 7.32–7.50 [m, 4H]; 7.65 [s, 1H, H-3]; 8.00 [s, 1H, H-6]; 8.38 [s, 1H, N = CH]; 9.62 [s, 1H, OH]; 11.08 [s, 1H, OH]; 11.69 [s, 1H, NH] ppm. HRMS (MALDI-TOF/TOF) *m/z* calculated for [M + H]$^+$ = 510.0360, found [M + H]$^+$ = 509.9880.

5.1.4.9. 5-[2-(Quinolin-2-ylmethylene)hydrazinocarbonyl]-2-chloro-4-[(4-fluorophenyl)methylthio]benzenesulfonamide (21). Starting with **2** (90 mg) and 2-quinolinecarboxaldehyde (38 mg) for 1 h, the title compound **21** was obtained (88 mg, 72 %): m.p. 251–252 °C; HPLC t_R = 23.71 min; R_f = 0.67 (A). IR (KBr) 3315, 3190 (N—H); 3078, 3044, 3009 (C_{Ar}-H); 2930 (CH_3); 1673 (N—H); 1580 (C═N); 1508 (C═C); 1344 (SO_2 *asym*); 1160 (SO_2 *sym*) cm^{-1}; ^{1}H NMR (500 MHz, DMSO-d_6, 100 °C): δ 4.38 [s, 2H, CH_2-S]; 7.07 [dd, $^3J_{HH}$ = 8.5 Hz, 2H, arom]; 7.26–7.53 [m, 5H, arom, NH_2]; 7.64 [t, $^3J_{HH}$ = 7.3 Hz, 1H, arom]; 7.71 [s, 1H, H-3]; 7.78 [t, $^3J_{HH}$ = 7.3 Hz, 1H, arom]; 7.98 [d, $^3J_{HH}$ = 7.8 Hz, 1H, arom]; 8.02–8.12 [m, 2H, arom]; 8.36 [d, $^3J_{HH}$ = 8.3 Hz, 1H, arom]; 8.43 [s, 1H, N = CH]; 12.11 [s, 1H, NH] ppm. HRMS (MALDI-TOF/TOF) *m/z* calculated for [M + H]$^+$ = 529.0571, found [M + H]$^+$ = 529.0235.

5.1.4.10. 2-Chloro-4-[(4-fluorophenyl)methylthio]-5-[2-(pyridin-4-ylmethylene)hydrazinecarbonyl]benzenesulfonamide (22). Starting with **2** (90 mg) and 4-pyridine carboxaldehyde (26 mg) for 1 h, the title compound **22** was obtained (105 mg, 95 %): m.p. 203–204 °C; HPLC t_R=18.62 min; R_f = 0.44 (A), R_f = 0.66 (B). IR (KBr) 3318, 3147 (N—H); 3053 (C_{Ar}-H); 2928, 2855 (CH_3); 1666 (N—H); 1583 (C═N); 1507 (C═C); 1310 (SO_2 *asym*); 1172 (SO_2 *sym*) cm^{-1}; ^{1}H NMR (500 MHz, DMSO-d_6, 100 °C): δ 4.37 [s, 2H, CH_2-S]; 7.08 [dd, $^3J_{HH}$ = 9 Hz, 2H, arom]; 7.28–7.56 [m, 4H, arom]; 7.70 [s, 1H, H-3]; 7.75 [s, 2H, NH_2]; 8.00 [s, 1H, H-6]; 8.31 [s, 1H, N = CH]; 8.71 [d, 2H, arom]; 12.19 [s, 1H, NH] ppm; ^{13}C NMR (125 MHz, 140 °C, DMSO-d_6): δ 37.1, 115.6, 115.7, 122.8, 129.0, 131.1, 131.2, 132.7, 133.0, 134.4, 138.9, 142.2, 143.7, 146.3, 146.8, 161.1, 163.0 ppm. HRMS (MALDI-TOF/TOF) *m/z* calculated for [M + H]$^+$ = 479.0415, found [M + H]$^+$ = 479.0136.

5.2. X-ray

Diffraction intensity data for **3** were collected on an IPDS 2T dual beam diffractometer (STOE & Cie GmbH, Darmstadt, Germany) at 120.0 (2) K with CuKa radiation of a microfocus X-ray source (GeniX 3D Mo High Flux, Xenocs, Sassenage, 50 kV, 0.6 mA, and λ = 1.54186 Å). Investigated crystals were thermostated under a nitrogen stream at 120 K using the CryoStream-800 device (Oxford CryoSystem, UK) during the entire experiment.

Data collection and data reduction were controlled by using the X-Area 1.75 program (STOE, 2015). Numerical absorption correction was performed by integration. The structure was solved using intrinsic phasing implemented in SHELXT and refined anisotropically using the program packages Olex2[39] and SHELX-2015.[40,41] Positions of the C—H hydrogen atoms were calculated geometrically taking into account isotropic temperature factors. All H-atoms were refined as riding on their parent atoms with the usual restraints, except H-atoms in –NH_2 groups, namely: in compound **3** atoms H1A and H1B, which were refined without constraints.

CCDC 2366980 contain the supplementary crystallographic data for this paper. The data can be obtained free of charge from The Cambridge Crystallographic Data Centre via www.ccdc.cam.ac.uk/structures.

5.3. CA inhibition assay

An Applied Photophysics (Oxford, UK) stopped-flow instrument has been used for assaying the CA-catalyzed CO_2 hydration activity.[42] Phenol red (at a concentration of 0.2 mM) has been used as indicator, working at the absorbance maximum of 557 nm, with 10 mM Hepes (pH 7.5) as buffer, 0.1 M Na_2SO_4 (for maintaining constant the ionic strength), following the CA-catalyzed CO_2 hydration reaction for a period of 10–100 s. The CO_2 concentrations ranged from 1.7 to 17 mM for the determination of the kinetic parameters and inhibition constants. For each inhibitor at least six traces of the initial 5–10 % of the reaction have been used for determining the initial velocity. The uncatalyzed rates were determined in the same manner and subtracted from the total observed rates. Stock solutions of inhibitor (1 mM) were prepared in distilled-deionized water with 10–20 % (v/v) DMSO (which is not inhibitory at these concentrations) and dilutions up to 0.1 nM were done thereafter with distilled-deionized water. Inhibitor and enzyme solutions were preincubated together for 15 min at room temperature prior to assay, in order to allow for the formation of E-I complex. The inhibition constants were obtained by non-linear last-squares methods using PRISM 3 and represent the mean from at least three different determinations.

5.4. Cell viability and cell cycle analysis

5.4.1. Cell culture

All chemicals, unless otherwise specified, were obtained from Sigma-Aldrich (St. Louis, MO, USA). The HCT-116 cell line was obtained from ATCC (ATCC-No: CCL-247), and the MCF-7, HeLa, and HaCaT cell lines were acquired from Cell Lines Services (Eppelheim, Germany). Cells were cultured in Dulbecco's modified Eagle's medium (DMEM)

supplemented with 10 % fetal bovine serum, 2 mM glutamine, 100 units/mL penicillin, and 100 μg/mL streptomycin. Cultures were maintained in a humidified atmosphere with 5 % carbon dioxide at 37 °C in an incubator (Heraceus, HeraCell).

5.4.2. MTT assay

The MTT (3-(4,5-dimethylthiazol-2-yl)-2,5-diphenyltetrazolium bromide) assay was used to evaluate cell viability. Cells were seeded at a density of 2×10^3 cells/well in 96-well plates and incubated for 24 h to allow cells to adhere. Cells were treated with the benzenesulfonamide derivatives at concentrations ranging from 1 to 100 μM (1, 10, 25, 50, and 100 μM) for a following 72-hour incubation. Compounds **9** and **19** were examined following a 24-, 48- and 72-hour incubation. Next, the MTT solution (0.5 mg/mL) was added to the medium, followed by a 2-hour incubation at 37 °C. Subsequently, cells were lysed with DMSO, and the absorbance of the formazan solution was measured at 550 nm using a plate reader (1420 Multilabel Counter, Victor, Jügesheim, Germany). The experiment was performed in triplicate, with results expressed as the mean ± SD from at least three independent experiments. The 4-parameter logistic (4PL) model was used in dose–response curve analysis to determine IC_{50} values. The concentration–response data were fitted to a 4-parameter logistic model described by the equation:

$$y = d + (a - d)/(1 + (x/c)\hat{}b),$$

where a and d are the maximum and minimum asymptotes, respectively; b is the Hill slope, which describes the steepness of the curve; c is the concentration at the infliction point.

5.4.3. Colony forming assay

MCF-7 cells were seeded at a density of 10^3 cells/well in 12-well plates. Cells were treated with compounds **9** and **19** for 24 h, after which the medium was replaced with DMEM medium. The cells were incubated for 2 weeks, exchanging the medium every 3 days. Following incubation, cells were fixed with methanol and stained with 0.5 % crystal violet solution. Colonies were counted and expressed as a percentage of the control.

5.4.4. Cell cycle analysis

The analysis of cell cycle distribution in MCF-7 cells following compounds **9** and **19** treatment was determined with flow cytometry. Cells were treated with compounds **9** and **19** (2.5, 5, and 10 μM) for 48 h and 72 h. For the analysis of the involvement of ERK in cell cycle arrest, cells were pre-treated with 1 μM U0126 for 1 h, followed by a 48-h incubation with compounds **9** and **19** (5 μM). Cells were fixed with 70 % ethanol for 24 h, after which RNAse (100 μg/mL, Invitrogen, Germany) and stained with propidium iodide (10 μg/mL, Invitrogen, Germany) for 30 min at RT. Analysis was performed with a FACSCalibur cytometer (BD), and with Flowing software (version 2.5).

5.5. Apoptosis assays

5.5.1. Annexin V staining

Apoptosis induction was analyzed with an Annexin V-PE Apoptosis Detection Kit I (BD Biosciences, Belgium) per the manufacturer's instructions. In order to determine concentration-dependent apoptosis induction, MCF-7 cells were treated with **9** and **19** (2.5, 5 and 10 μM) for 72. To evaluate the involvement of ERK inhibition in apoptosis induction, cells were pre-treated with 1 μM U0126 for 1 h, followed by a 72-h incubation with **9** and **19** (10 μM). Cells were collected and stained in an Annexin-binding buffer containing Annexin V-phycoerythrin (PE) and 7-amino-actinomycin (7-AAD) for 30 min in the dark at RT. Analysis was performed with a FACSCalibur cytometer (BD), and with Flowing software (version 2.5).

5.5.2. Caspase activation analysis

Caspase activity analysis was carried out with the FLICA Apoptosis Detection Kit (Immunochemistry Technologies) per the manufacturer's instructions. MCF-7 cells were treated with compounds **9** and **19** for 48 h, cells were collected, and the cell suspension was incubated in a buffer containing the caspase inhibitor, i.e., a carboxyfluorescein-labeled fluoromethyl ketone peptide for 1 h in a CO_2 incubator. Following the washing of cells with the Kit's washing buffer, fluorescence was measured with flow cytometry (BD FACSCalibur), and analyzed with Flowing software (version 2.5). Caspase activity was assessed as the fluorescence intensity of the caspase inhibitor bound to the active caspases.

5.5.3. Mitochondrial membrane permeability assessment

The assessment of changes in mitochondrial membrane potential (Δψm) was performed with the BD™ MitoScreen Kit (BD Biosciences, Belgium) utilizing the lipophilic fluorochrome, JC-1 (5,5′,6,6′-tetrachloro-1,1′,3,3′- tetraethylbenzimidazolcarbocyanine iodide). The assay was carried out according to the manufacturer's instructions. Cells were incubated with compounds **9** and **19** (2.5, 5, and 10 μM) for 48 h, after which cells were collected and incubated with JC-1 working solution for 15 min in a CO_2 incubator. Following the washing of cells with the Kit's washing solution, cells were analyzed with flow cytometry (BD FACSCalibur), and Flowing software (version 2.5). The population with decreased fluorescence in the FL-2 channel was analyzed and presented as the percentage of cells with depolarized Δψm.

5.6. AlphaScreen analysis

The activation of ERK1/2 was analyzed using the bead-based amplified luminescent proximity homogeneous assay (AlphaScreen). The assay was used to detect phosphorylated ERK (p-ERK 1/2 (Thr202/Tyr204)) and total ERK 1/2 (SureFire, PerkinElmer, Rodgau, Germany). Cells were serum-starved overnight, then treated with compounds **9** and **19** for 24 h at 5 % CO_2 at 37 °C. To determine the influence of ERK inhibition on the activity of benzenesulfonamides, cells were pre-treated with U0126 (1 μM) for 1 h, followed by the treatment of cells with compounds **9** and **19** for 24 h. Following incubation, the medium was discarded, 50 μL of SureFire lysis buffer was added, and the plates were agitated on a plate shaker for 10 min at approximately 350 rpm at RT. The p-ERK and total ERK levels were detected according to the manufacturer's instructions. For p-ERK analysis, 4 μL of the cell lysate was added to a 384-well plate (Proxiplate, PerkinElmer), followed by 7 μL of the reaction mix (containing reaction buffer, activation buffer, donor, and acceptor beads) and a 2 h incubation at RT. To analyze total ERK levels, 4 μL of the cell lysate was added to a 384-well plate, and then 5 μL of the acceptor mix (containing the reaction buffer, activation buffer, and acceptor beads) was added. Following a 2 h incubation at RT, 2 μL of donor mix (containing donor beads in dilution buffer) and a further 2 h incubation at RT. Plates designated for p-ERK and total ERK analysis were read with an Envision multilabel reader (PerkinElmer) with standard AlphaScreen settings, and the intensity of the luminescent signals was detected. The p-ERK levels were normalized to total ERK levels to determine the changes in p-ERK activity.

5.7. Statistical analysis

Statistical analysis was performed with GraphPad Prism 5.0 (GraphPad software). Values are presented as the means ± SD, based on a minimum of three independent experiments. The differences between the control and experimental samples were analyzed by one-way ANOVA with Tukey's post hoc tests. A p-value < 0.05 was considered statistically significant.

CRediT authorship contribution statement

Beata Żołnowska: Writing – review & editing, Writing – original draft, Visualization, Supervision, Methodology, Investigation, Data curation, Conceptualization. **Jarosław Sławiński:** Writing – review & editing, Supervision, Methodology. **Jarosław Chojnacki:** Writing – review & editing, Supervision, Methodology. **Andrea Petreni:** Investigation, Data curation. **Claudiu T. Supuran:** Writing – review & editing, Visualization, Methodology, Data curation. **Anna Kawiak:** Writing – review & editing, Writing – original draft, Visualization, Methodology, Investigation, Data curation.

Declaration of competing interest

The authors declare that they have no known competing financial interests or personal relationships that could have appeared to influence the work reported in this paper.

Acknowledgments

"The financial support to maintenance of research facilities used in these studies from Gdańsk University of Technology by the DEC-2/2021/IDUB/V.6/Si grant under the SILICIUM SUPPORTING CORE R&D FACILITIES – "Excellence Initiative - Research University" program is gratefully acknowledged".

Appendix A. Supplementary data

Supplementary data to this article can be found online at https://doi.org/10.1016/j.bmc.2024.117958.

Data availability

Data will be made available on request.

References

1. Galluzzi L, Vitale I, Aaronson SA, et al. Molecular mechanisms of cell death: recommendations of the nomenclature committee on cell death. *Cell Death Differ*. 2018;25:486–541.
2. Carneiro BA, El-Deiry WS. Targeting apoptosis in cancer therapy. *Nat Rev Clin Oncol*. 2020;17:395–417.
3. Giaquinto AN, Sung H, Miller KD, Kramer JL, Newman LA, Minihan A, Jemal A, Siegel RL. Breast cancer statistics, 2022. *CA A Cancer J Clin*. 2022;72:524–541.
4. Yoon S, Seger R. The extracellular signal-regulated kinase: Multiple substrates regulate diverse cellular functions. *Growth Factors*. 2006;24:21–44.
5. Dhillon AS, Hagan S, Rath O, Kolch W. MAP kinase signalling pathways in cancer. *Oncogene*. 2007;26:3279–3290.
6. Drew J. Drug discovery: a historical perspective. *Science*. 2000;287:1960–1964.
7. Kaur IP, Smitha R, Aggarwal D, Kapil M. Acetazolamide: future perspective in topical glaucoma therapeutics. *Int J Pharm*. 2002;248:1–14.
8. Supuran CT, Conroy CW, Maren TH. Carbonic anhydrase inhibitors: Synthesis and inhibitory properties of 1,3,4-thiadiazole-2,5-bissulfonamide. *Eur J Med Chem*. 1996;31:843–846.
9. Wouters J, Michaux C, Durant F, Dogné JM, Delarge J, Masereel B. Isosterism among analogues of torasemide: conformational, electronic and lipophilic properties. *Eur J Med Chem*. 2000;35:923–929.
10. Noble S, Goa KL. Amprenavir: a review of its clinical potential in patients with HIV infection. *Drugs*. 2000;60:1383–1410.
11. Scozzafava A, Owa T, Mastrolorenzo A, Supuran CT. Anticancer and antiviral sulfonamides. *Curr Med Chem*. 2003;10:925–953.
12. Das R, Tambe G, Shard A. Sulfonamides as tyrosine kinase modulators – a promising class of anticancer agents. *Results Chem*. 2023;5, 100950.
13. Supuran CT. A simple yet multifaceted 90 years old, evergreen enzyme: carbonic anhydrase, its inhibition and activation. *Bioorg Med Chem Lett*. 2023;93, 129411.
14. Bekku S, Mochizuki H, Yamamoto T, Ueno H, Takayama E, Tadakuma T. Expression of carbonic anhydrase I or II and correlation to clinical aspects of colorectal cancer. *Hepatogastroenterology*. 2000;47:998–1001.
15. Swietach P, Patiar S, Supuran CT, Harris AL, Vaughan-Jones RD. The role of carbonic anhydrase 9 in regulating extracellular and intracellular ph in three-dimensional tumor cell growths. *J Biol Chem*. 2009;284:20299–20310.
16. Morgan PE, Pastoreková S, Stuart-Tilley AK, Alper SL, Casey JR. Interactions of transmembrane carbonic anhydrase, CAIX, with bicarbonate transporters. *Am J Physiol Cell Physiol*. 2007;293:738–748.
17. McIntyre A, Patiar S, Wigfield S, et al. Carbonic anhydrase IX promotes tumor growth and necrosis in vivo and inhibition enhances anti-VEGF therapy. *Clin Cancer Res*. 2012;18:3100–3111.
18. Xiao-Qun Z, Xian-Li M, Ariffin NS. The potential of carbonic anhydrase enzymes as a novel target for anti-cancer treatment. *Eur J Pharmacol*. 2024;976:17667.
19. Ronca R, Supuran CT. Carbonic anhydrase IX: An atypical target for innovative therapies in cancer. *Biochim Biophys Acta*. 2024;1879, 189120.
20. Supuran CT. Carbonic anhydrase inhibitors. *Bioorg Med Chem Lett*. 2010;20:3467–3474.
21. Chafe SC, Vizeacoumar FS, Venkateswaran G, et al. Genome-wide synthetic lethal screen unveils novel CAIX-NFS1/xCT axis as a targetable vulnerability in hypoxic solid tumors. *Sci Adv*. 2021;7:eabj0364.
22. McDonald PC, Chafe SC, Supuran CT, Dedhar S. Cancer therapeutic targeting of hypoxia induced carbonic anhydrase IX: from bench to bedside. *Cancers (Basel)*. 2022;14:3297.
23. Verma G, Marella A, Shaquiquzzaman M, Akhtar M, Ali MR. A review exploring biological activities of hydrazones. *J Pharm Bioallied Sci*. 2014;6:69–80.
24. Rollas S, Kucukguzel SG. Biological activities of hydrazone derivatives. *Molecules*. 2007;12:1910–1939.
25. Singh RK, Singh AK, Siddiqui S, et al. Synthesis, molecular structure, spectral analysis and cytotoxic activity of two new aroylhydrazones. *J Mol Struct*. 2017;1135:82–97.
26. Ahmed MF, El-Haggar R, Almalki AH, et al. Novel hydrazone-isatin derivatives as potential EGFR inhibitors: Synthesis and in vitro pharmacological profiling. *Arch Pharm (Weinheim)*. 2023;356.
27. Abdel-Aziz AA, El-Azab AS, AlSaif NA, Obaidullah AJ, Al-Obaid AM, Al-Suwaidan IA. Synthesis, potential antitumor activity, cell cycle analysis, and multitarget mechanisms of novel hydrazones incorporating a 4-methylsulfonylbenzene scaffold: a molecular docking study. *J Enzyme Inhib Med Chem*. 2021;36:1521–1539.
28. Sahu G, Banerjee A, Samanta R, et al. Water-soluble dioxidovanadium(V) complexes of aroylhydrazones: DNA/BSA interactions, hydrophobicity, and cell-selective anticancer potential. *Inorg Chem*. 2021;60:15291–15309.
29. Bray F, Laversanne M, Sung H, et al. GLOBOCAN estimates of incidence and mortality worldwide for 36 cancers in 185 countries. *CA Cancer J Clin*. 2022;74:229–263.
30. Carta F, Vullo D, Osman SM, AlOthman Z, Supuran CT. Synthesis and carbonic anhydrase inhibition of a series of SLC-0111 analogs. *Bioorg Med Chem*. 2017;25:2569–2576.
31. Wu TY, Cho TY, Lu CK, Liou JP, Chen MC. Identification of 7-(4′-Cyanophenyl) indoline-1-benzenesulfonamide as a mitotic inhibitor to induce apoptotic cell death and inhibit autophagy in human colorectal cancer cells. *Sci Rep*. 2017;7:12406.
32. Meng LH, Kohn KW, Pommier Y. Dose-response transition from cell cycle arrest to apoptosis with selective degradation of Mdm2 and p21WAF1/CIP1 in response to the novel anticancer agent, aminoflavone (NSC 686288). *Oncogene*. 2007;26:4806–4816.
33. Fulda S, Gorman AM, Hori O, Samali A. Cellular stress responses: Cell survival and cell death. *Int. J. Cell Biol*. 2010;2010, 214074.
34. Kawiak A, Kostecka A. Regulation of Bcl-2 family proteins in estrogen receptor-positive breast cancer and their implications in endocrine therapy. *Cancers (Basel)*. 2022;14:279.
35. Fulda S, Debatin KM. Extrinsic versus intrinsic apoptosis pathways in anticancer chemotherapy. *Oncogene*. 2006;25:4798–4811.
36. Sugiura R, Satoh R, Takasaki T. ERK: a double-edged sword in cancer. ERK-dependent apoptosis as a potential therapeutic strategy for cancer. *Cells*. 2021;10:2509.
37. Lee M, Young Kim S, Kim J, Kim HS, Kim SM, Kim EJ. Mitogen-activated protein kinase phosphatase-1 inhibition and sustained extracellular signal-regulated kinase 1/2 activation in camptothecin-induced human colon cancer cell death. *Cancer Biol Ther*. 2013;14:1007–1015.
38. Cumaoglu A, Dayan S, Agkaya AO, Ozkul Z, Ozpozan NK. Synthesis and pro-apoptotic effects of new sulfonamide derivatives via activating p38/ERK phosphorylation in cancer cells. *J Enzyme Inhib Med Chem*. 2015;30:413–419.
39. Dolomanov OV, Bourhis LJ, Gildea RJ, Howard JAK, Puschmann H. *J Appl Cryst*. 2009;42:339–341.
40. Sheldrick GM. SHELXT – integrated space-group and crystal-structure determination. *Acta Cryst A*. 2015;71:3–8.
41. Sheldrick GM. Crystal structure refinement with SHELXL. *Acta Cryst. C*. 2015;71:3–8.
42. Khalifah RG. The carbon dioxide hydration activity of carbonic anhydrase. I. Stop-flow kinetic studies on the native human isoenzymes B and C. *J Biol Med*. 1971;246:2561–2573.